

---

# Capsize criteria for ship models with memory-dependent hydrodynamics and random excitation

BY C. JIANG<sup>1</sup>, A. W. TROESCH<sup>2</sup> AND S. W. SHAW<sup>3</sup>

<sup>1</sup>*Band, Lavis and Associates, Severna Park, MD 21146, USA*

<sup>2</sup>*Department of Naval Architecture and Marine Engineering,  
University of Michigan, Ann Arbor, MI 48109-2145, USA*

<sup>3</sup>*Department of Mechanical Engineering, Michigan State University,  
East Lansing, MI 48824-1226, USA*

The large-amplitude rolling and capsize dynamics of vessels in random beam seas are investigated using a nonlinear single-degree-of-freedom model. Included in this model are three types of damping moments—the usual effects that are treated as linear and quadratic in the roll velocity, plus a frequency-dependent effect that captures the dissipation of energy caused by the generation of waves radiated away from the rolling vessel. The description of this type of damping requires a history-dependent term in the equations of motion. This memory effect prevents a straightforward application of the standard Melnikov method for determining capsize criteria. In this work, the Melnikov function and phase-space transport techniques are extended to derive a criterion for capsizing that can be applied to analytical models with this type of damping. Using these theoretical results, we obtain a closed-form asymptotic expression for a critical significant wave height, and this criterion is evaluated using simulation studies for a realistic set of vessel parameters.

**Keywords:** ship capsize; nonlinear random processes;  
global stability; Melnikov method

---

## 1. Introduction

The nonlinear behaviour of ship motion leading to capsize has been extensively studied by many authors using a variety of mathematical models for the ship and the sea state. The dynamic models proposed for ship dynamics range from those describing the full six degrees of freedom to those with only a single degree of freedom (typically roll). Examples of research using multi-degree-of-freedom models are given by Vassalos & Spyrou (1990), Falzarano & Zhang (1993), Umeda & Renilson (1994), Spyrou & Umeda (1995), Spyrou (1996) and Vassalos *et al.* (1999). A reduction in the degrees of freedom results in more idealized models, and often allows for a more rigorous analysis that yields mathematical results in terms of the system parameters. Such reductions can, in many cases, be mathematically justified using invariant manifold theory, as demonstrated by Chen *et al.* (1999). The work described in this paper is based upon such a single-degree-of-freedom (SDOF) model, representing a rolling vessel in random beam seas with memory-dependent hydrodynamics.

Many methods have been developed to analyse nonlinear ship rolling for SDOF models. Examples of the more successful of these are the regular perturbation method (Wright & Marshfield 1980; Cardo *et al.* 1981, 1984), the multiple scales method (Nayfeh & Khdeir 1986*a,b*), the method of averaging (Nayfeh 1973; Cardo *et al.* 1981, 1984), the harmonic balance method (Wright & Marshfield 1980; Senjanović 1994) and numerical simulation methods (Thompson 1989*a,b*, 1990; Virgin 1987, 1989). The first three methods are restricted to weakly nonlinear systems, which are not representative of large-amplitude roll motion that can lead to capsizing. In order to achieve convergence for the harmonic balance method, many terms are needed, and this often makes the resulting algebraic equations prohibitively complicated. Simulation results are very powerful, especially when combined with an understanding of the underlying phase space, as done in the ground-breaking work of Thompson and his co-workers (Thompson 1989*a,b*, 1990; Virgin 1987, 1989), and more recently by Spyrou (1996). A comprehensive review of the mechanics of ship capsizing using global geometrical techniques is given by Thompson (1997). These simulation-based methods offer insight, but do not yield analytical results that allow for *a priori* prediction of the effects of system parameters on the response of the ship to various types of excitation. In addition, all of the above methods are applicable for deterministic wave excitation but have not been applied to extreme ship motions under stochastic excitation. Some analytical methods have been used for analysing roll dynamics in random seas, including the stochastic averaging method, introduced by Roberts (1982) and Roberts & Dacunha (1985) for application to ship motions, and its extension by Huang *et al.* (1994) to a system with a fifth-order polynomial restoring moment.

More recently, combined geometric/analytical methods have been applied to the problem of nonlinear ship dynamics. Instead of directly solving the nonlinear differential equations, these methods emphasize the qualitative behaviour of the system, and often allow for analytical estimates of important features of large-amplitude responses. One of the more popular analytic techniques of this type is the Melnikov method, which can predict parameter conditions under which capsizing is possible. This approach, which is restricted to certain classes of system models, describes conditions under which solutions of the model equations can be transported from one region of the system phase space (e.g. safety) to another (e.g. capsizing). The works of Wiggins (1990, 1992) describe the basic theory and an important general application of Melnikov's method, called *chaotic transport theory*. A significant result from this theory is that the rate at which solutions are transported out of the safe regions, called the *phase-space flux rate*, can be calculated from the Melnikov function. These ideas, originally developed for deterministic excitation, were applied to the capsizing problem in harmonic waves by Falzarano *et al.* (1992). The method has been extended to systems that have random excitation (Frey & Simiu 1993) and applied to the problem of ship capsizing in random beam seas (Hsieh *et al.* 1994; Jiang *et al.* 1996).

In all the above methods, the coefficients used to model hydrodynamic loads are taken to be constants. However, in general, the hydrodynamic coefficients are frequency dependent. For excitations of multiple or even infinite number of frequencies (e.g. random excitation), it is common to approximate the hydrodynamic effect by simply using a coefficient computed at a particular frequency of interest. Another approach to this problem, and the one employed in the present study, is to model the

frequency-dependent term as the response of an auxiliary dynamical system. Holappa & Falzarano (1999) considered the extended state space associated with such a model, including nonlinear rolling effects and frequency-dependent coefficients. Using numerical integration, they found that acceptable results could be obtained for some cases by using constant hydrodynamic coefficients evaluated at a frequency based upon the zero crossing period of the sea spectrum. They did not consider extreme motions leading to capsize.

In this paper, we consider the frequency dependence of the system's hydrodynamic coefficients and apply Melnikov's method to the extended dynamical system that includes the auxiliary system. The results are obtained for the case of random sea states. The paper is organized as follows. We begin with a review of the basic system model, in which we incorporate memory-dependent radiation effects in the nonlinear differential equations, valid for large-amplitude roll dynamics. Attention is paid to the relationships between the frequency and time-domain descriptions of these radiation terms. Next, the Melnikov function for this system model with random excitation is derived and is described in terms of its statistical properties. These results are then linked to the likelihood of capsize through a measure of the rate of phase-space transport. These results are used to study the effects of the damping model on the capsize criterion. Extensive simulations are used to verify the analytical results, and the paper closes with some conclusions.

## 2. The model for rolling motion

### (a) *The basic model*

Ship rolling behaviour can be represented by the following SDOF equation (see, for example, Jiang *et al.* 1994):

$$(I_{44} + A_{44}(\omega))\ddot{\phi} + B_{44}(\omega)\dot{\phi} + B_{44q}(\omega)\dot{\phi}|\dot{\phi}| + \Delta(C_0 + C_1\phi + C_3\phi^3 + \dots) = F(\tau), \quad (2.1)$$

where  $\phi$  is the roll angle in an absolute reference frame,  $(\dot{\phantom{x}}) = d/d\tau$ ,  $I_{44}$  is the moment of inertia of the dry vessel with respect to an axis along an assumed roll centre,  $F(\tau)$  is the moment due to incident waves with respect to the same axis,  $A_{44}(\omega)$  is the added mass coefficient,  $B_{44}(\omega)$  and  $B_{44q}(\omega)$  are linear and quadratic damping coefficients, respectively,  $\Delta$  is the displacement of the vessel,  $C_1$  and  $C_3$  are linear and nonlinear coefficients of the restoring arm, and  $C_0$  the bias moment which can arise due to wind, cargo, vessel damage or the pull of a fishing net. (Note that the nonlinear restoring moment is assumed to be valid for large angles, that is, it is derived from a curve fit or a series expansion.)

$A_{44}(\omega)$  and  $B_{44}(\omega)$  are frequency dependent because of the presence of the free surface. For a single sinusoidal excitation  $F(\tau)$  and sinusoidal response, they take values corresponding to the excitation frequency. Only in this case can (2.1) exactly describe the linear ship roll hydrodynamics (Ogilvie 1964). If the excitation is not purely sinusoidal, e.g. for random excitation,  $A_{44}(\omega)$  and  $B_{44}(\omega)$  are no longer constant and (2.1) is an approximation (see Takagi *et al.* 1984; Jiang *et al.* 1996). For excitation represented by narrow-banded spectra,  $A_{44}(\omega)$  and  $B_{44}(\omega)$  may be evaluated at the dominant excitation frequency, say,  $\omega_z$  (see, for example, Esparza & Falzarano 1993; Holappa & Falzarano 1999). For excitations with wide-banded spectra, the values at the roll natural frequency may be better.

(b) *A frequency-dependent model for random excitation*

To improve this frequency-domain description, a modified model is needed—one that can be represented in the time domain. In linear hydrodynamics, the ship hydrodynamic forces can be viewed as the output of a linear system with the wave elevation ( $\zeta(\tau)$ ) and roll motion ( $\phi(\tau)$ ,  $\dot{\phi}(\tau)$  and  $\ddot{\phi}(\tau)$ ) as its inputs. The output corresponding to  $\zeta(\tau)$  is the so-called external excitation  $F(\tau)$ , which can be related to  $\zeta(\tau)$  in the frequency domain as follows:

$$S_f^+(\omega) = |F_{\text{roll}}(\omega)|^2 S_\zeta^+(\omega), \tag{2.2}$$

where  $F_{\text{roll}}(\omega)$  is the roll moment amplitude per unit wave height,  $S_\zeta^+(\omega)$  and  $S_f^+(\omega)$  are the wave elevation spectrum and the wave-induced roll moment spectrum, respectively.  $F_{\text{roll}}(\omega)$  depends on frequency as well as ship geometry. The wave elevation  $\zeta(\tau)$  is usually assumed to a stationary ergodic Gaussian stochastic process. One accepted model is the ISSC two-parameter spectrum,

$$S_\zeta^+(\omega) = 0.11 H_s^2 \frac{\omega_z^4}{\omega^5} \exp\left(-0.44 \left(\frac{\omega_z}{\omega}\right)^4\right), \tag{2.3}$$

where  $H_s$  is the significant wave height and  $\omega_z$  is the characteristic wave frequency.

The hydrodynamic moment associated with  $\phi(\tau)$  is the ‘hydrostatic’ restoring moment, that is,  $\Delta(C_0 + C_1\phi + C_3\phi^3 + \dots)$  in (2.1), the characteristics of which depend only upon ship geometry. The hydrodynamic reaction moment due to  $\dot{\phi}(\tau)$  and  $\ddot{\phi}(\tau)$  is conceptually identified with the radiation, i.e. forced motion, problem. Mathematically, the linear radiation force can be taken as the sum of a succession of impulse responses. Following Ogilvie (1964), the time-domain ship rolling equation is

$$\begin{aligned} (I_{44} + A_{44}(\infty))\ddot{\phi} + B_{44}(\infty)\dot{\phi} + \int_0^\tau K(\tau - u)\dot{\phi}(u) du \\ + B_{44q}(\omega)\dot{\phi}|\dot{\phi}| + \Delta(C_0 + C_1\phi + C_3\phi^3 + \dots) = F(\tau), \end{aligned} \tag{2.4}$$

where  $A_{44}(\infty)$  is the hydrodynamic added mass coefficient evaluated at the infinite frequency limit and  $K(\tau)$  is the hydrodynamic rolling moment due to impulse roll velocity. The integral of the  $K(\tau)$  term is usually called the memory function because it represents how roll-radiation moments depend on the history of rolling velocity. Modelled in this way, the hydrodynamic forces (moments) change instantaneously with  $\phi(\tau)$  and  $\ddot{\phi}(\tau)$ , but the influence from  $\dot{\phi}(\tau)$  is cumulative and will be present for sometime before it dies out.

The time- and frequency-domain descriptions of rolling motion are connected to each other through the following relation (Ogilvie 1964; Takagi *et al.* 1984):

$$K(\tau) = -\frac{2}{\pi} \int_0^\infty \omega (A_{44}(\omega) - A_{44}(\infty)) \sin(\omega\tau) d\omega \tag{2.5}$$

$$= \frac{2}{\pi} \int_0^\infty (B_{44}(\omega) - B_{44}(\infty)) \cos(\omega\tau) d\omega. \tag{2.6}$$

To obtain a time-domain description like (2.4), the hydrodynamic problem may be solved in the frequency domain for a range of frequencies. This may be done by applying commercially available linear hydrodynamic programs, e.g. SHIPMO.BM (Beck

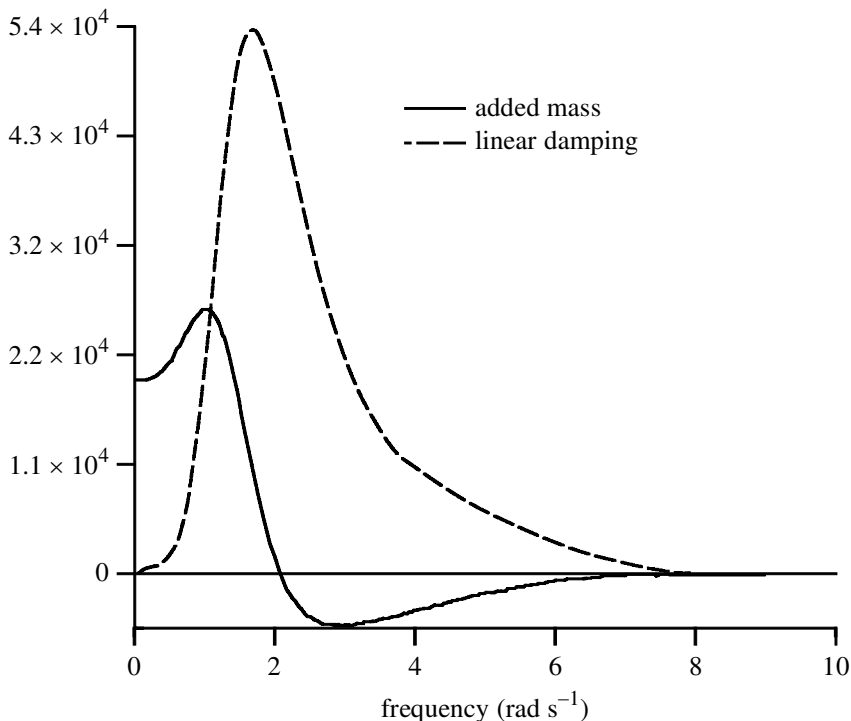


Figure 1. The added mass ( $A_{44}(\omega) - A_{44}(\infty)$ ) and linear damping ( $B_{44}(\omega) - B_{44}(\infty)$ ) coefficients obtained from SHIPMO for *Patti-B*. The units are  $\text{N m}^{-1} \text{s}^{-2}$  for  $A_{44}$  and  $\text{N m}^{-1} \text{s}^{-1}$  for  $B_{44}$ .  $A_{44}(\infty) = 1.441 \times 10^6$  and  $B_{44}(\infty) = 0$ .

& Troesch 1990). The results for *Patti-B*, a fishing vessel, are shown in figure 1 and the corresponding  $K(t)$ , obtained from (2.6), is shown in figure 2. It should be noted that  $A_{44}(\omega)$  and  $B_{44}(\omega)$  are both even functions of  $\omega$ . Therefore,  $A_{44}(\omega) - A_{44}(\infty)$  and  $B_{44}(\omega) - B_{44}(\infty)$  are also even and the negative frequency domain is omitted in figure 1. The Fourier transform of memory function  $K(\tau)$  is related to the hydrodynamic coefficients as follows (Takagi *et al.* 1984):

$$\mathcal{K}(\omega) = \frac{1}{2\pi} [B_{44}(\omega) - B_{44}(\infty) + i\omega(A_{44}(\omega) - A_{44}(\infty))], \quad (2.7)$$

where the  $1/2\pi$  may not be needed, depending on the definition of the Fourier transform.

The quadratic damping coefficient  $B_{44q}(\omega)$  in (2.1) and (2.4) is found by experimental tests. While it may have some small frequency dependence (Himeno 1981), in this work it is treated as constant. The linear roll damping goes to zero as the frequency goes to infinity and roll velocity is bounded, thereby eliminating the term  $B_{44}(\infty)\dot{\phi}$  in (2.4). Note also that the added mass term tends to a non-zero constant as the frequency goes to infinity (figure 1 shows  $A_{44}(\omega) - A_{44}(\infty)$  instead of  $A_{44}(\omega)$ ). From causality, it is understood that the impulse response function  $K(\tau)$  is zero for  $\tau < 0$ . Since  $K(\tau < 0) = 0$  and  $\dot{\phi}(\tau < 0) = 0$ , the integration limit in (2.4) can be

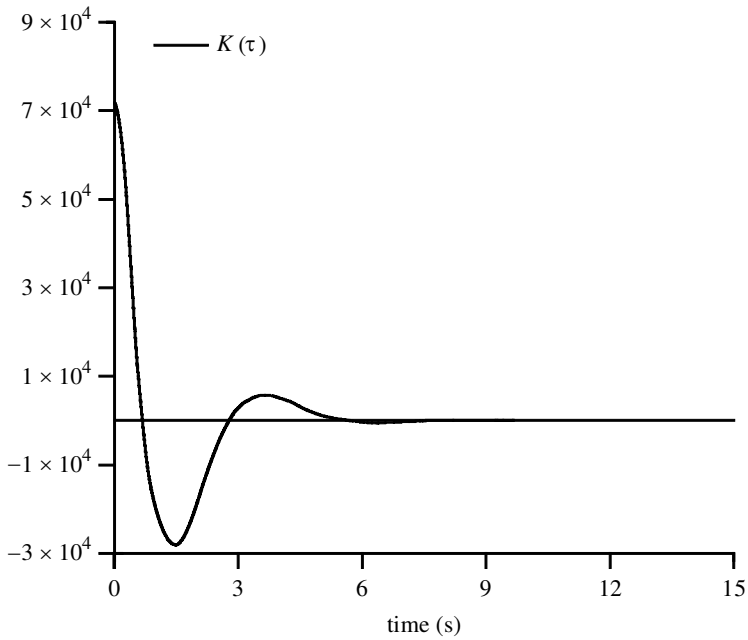


Figure 2. The impulse response  $K(\tau)$  function calculated from the inverse cosine transform of  $B_{44}(\omega) - B_{44}(\infty)$ . The unit is  $\text{N m}^{-1}$ .  $B_{44}(\infty) = 0$ .

expanded to  $(-\infty, \infty)$  and (2.4) is rewritten as

$$(I_{44} + A_{44}(\infty))\ddot{\phi} + \int_{-\infty}^{\infty} K(\tau - u)\dot{\phi}(u) du + B_{44q}(\omega)\dot{\phi}|\dot{\phi}| + \Delta(C_0 + C_1\phi + C_3\phi^3 + \dots) = F(\tau). \quad (2.8)$$

To distinguish this from the constant coefficient differential equation, equation (2.8) is called the integro-differential equation. For the purpose of comparison with previously published results (Hsieh *et al.* 1994; Jiang *et al.* 1996), we simplify the restoring moment by taking  $C_i = 0$  for  $i > 3$ . However, the method introduced here is able to handle any form of angle-dependent hydrostatic restoring moment.

(c) *Scaling the equations of motion*

In large-amplitude roll, nonlinear effects in the restoring moment can easily dominate the behaviour. The method used in this work is a global perturbation method that allows one to predict certain features of such nonlinear behaviour. It is based on determining the effects that relatively small damping and excitation have on the overall nonlinear system behaviour. In fact, as shown below, the terms in the roll equation of motion scale exactly as needed for application of this method.

To compare the relative orders of the various terms in the roll equation, we rewrite the usual roll differential equation (2.1) and the history-dependent integro-differential equation (2.8) in non-dimensional forms, as follows:

$$\ddot{x}(t) + \epsilon\delta_1\dot{x}(t) + \epsilon\delta_2\dot{x}(t)|\dot{x}(t)| + \delta + x(t) - \alpha x^3(t) = \epsilon f(t) \quad (2.9)$$

Table 1. List of parameters for Patti-B, a 22.9 m, 238 t fishing boat

| parameter                   | dimensional value                                      | parameter                       | dimensional value                      |
|-----------------------------|--|---------------------------------|--|
| $C_1$                       | 0.214 m  | $C_3$                           | -0.671 m                               |
| $\Delta$                    | $0.237 \times 10^7$ N                                  | $F_{\text{roll}}(\omega = 0.7)$ | $0.301 \times 10^4$ N m <sup>-1</sup>  |
| $I_{44} + A_{44}(\omega_n)$ | $0.147 \times 10^7$ kg m <sup>-2</sup>                 | $I_{44} + A_{44}(\infty)$       | $0.144 \times 10^7$ kg m <sup>-2</sup> |
| $\omega_n$ of (2.9)         | 0.587 rad s <sup>-1</sup>                              | $\omega_n$ of (2.10)            | 0.593 rad s <sup>-1</sup>              |
| $B_{44}(\omega_n)$          | $0.321 \times 10^4$ kg m <sup>-2</sup> s <sup>-1</sup> | $K(t) _{\text{maximum}}$        | $0.718 \times 10^5$ N m <sup>-1</sup>  |
| $B_{44}(\omega = 0.7)$      | $0.548 \times 10^4$ kg m <sup>-2</sup> s <sup>-1</sup> | $B_{44q}$                       | $0.988 \times 10^5$ kg m <sup>-2</sup> |

and

$$\ddot{x}(t) + \epsilon \int_{-\infty}^{\infty} \delta_m(t-u)\dot{x}(u) du + \epsilon\delta_2\dot{x}(t)|\dot{x}(t)| + \delta + x(t) - \alpha x^3(t) = \epsilon f(t), \quad (2.10)$$

where

$$\begin{aligned}
 x &= \phi, & t &= \omega_n \tau, & (\dot{\phantom{x}}) &= \frac{d}{dt}, \\
 \omega_n &= \sqrt{\frac{C_1 \Delta}{I_{44} + A_{44}}}, & \Omega &= \frac{\omega}{\omega_n}, \\
 \epsilon\delta_1 &= \frac{B_{44}\omega_n}{C_1 \Delta}, & \epsilon\delta_m(t) &= \frac{K(t)\omega_n^2}{C_1 \Delta} = \frac{K(t)}{I_{44} + A_{44}}, & \epsilon\delta_2 &= \frac{B_{44q}}{I_{44} + A_{44}}, \\
 \delta &= \frac{C_0}{C_1}, & \alpha &= \frac{-C_3}{C_1}, & \epsilon f(t) &= \frac{F(\tau)}{C_1 \Delta}.
 \end{aligned}$$

Note that  $A_{44}$  in (2.9) can be taken as  $A_{44} = A_{44}(\omega_n)$  or  $A_{44} = A_{44}(\omega_z)$ , and that  $A_{44} = A_{44}(\infty)$  for (2.10). The quadratic damping coefficient  $B_{44q}(\omega)$  is the same for both cases. The various coefficients for the Patti-B are listed in table 1. Compared with the added mass and linear restoring moment terms, which are of order 1, the nonlinear restoring coefficient  $\alpha$  is 3.14, the external excitation amplitude per unit wave height at a typical frequency is  $F_{\text{roll}}(\omega = 0.7) = 0.006$  and the quadratic damping coefficient  $\epsilon\delta_2$  is 0.067. The maximum value of the memory function  $\epsilon\delta_m(t)|_{\text{maximum}}$  is 0.050 for the integro-differential system (equation (2.10)), while the constant linear damping coefficient  $\epsilon\delta_1$  is 0.004 for the usual differential equation model given in (2.9). Therefore, the use of  $\epsilon$  as a scaling parameter for the damping and wave excitation terms is justified.

### 3. A capsize criterion for models with memory-dependent hydrodynamic forces

(a) The system phase space and its safe basin

It is convenient to express (2.10) in first-order form, as follows:

$$\dot{x}(t) = y(t), \tag{3.1}$$

$$\dot{y}(t) = -\delta - x(t) + \alpha x^3(t) + \epsilon \left( \int_{-\infty}^{\infty} \delta_m(t-u)y(u) du - \delta_2 y(t)|y(t)| + f(t) \right). \tag{3.2}$$

Note that (3.1) and (3.2) represent an integrable Hamiltonian system with some small perturbations terms (Wiggins 1990). The unperturbed system ( $\epsilon = 0$ )

$$\dot{x}(t) = y(t), \quad (3.3)$$

$$\dot{y}(t) = -\delta - x(t) + \alpha x^3(t) \quad (3.4)$$

is a conservative two-dimensional system with solutions as shown in the  $(x, y)$  phase planes given in figures 3 and 4. Except for some special cases (Falzarano *et al.* 1992; Huang *et al.* 1994), equations (3.3) and (3.4) must be solved numerically. For the symmetric unbiased system ( $\delta = 0$ ) shown in figure 3, the two saddle points, corresponding to the angles of vanishing stability, are connected by two symmetrical orbits known as heteroclinic orbits (shown as dashed lines). We use  $y_0^+(t)$  and  $y_0^-(t)$  to denote the ordinates of the upper branch and the lower branch, respectively, of these orbits in the phase plane as functions of time. Motions taking place inside the region enclosed by the heteroclinic orbits are bounded and safe, in terms of capsizing. This region is called the *safe basin* of the unperturbed system, and the heteroclinic orbits are the *basin boundaries*. Motions outside of this region lead to capsizing. In the asymmetric biased system shown in figure 4, the two saddle points are not connected but the left saddle point is connected to itself by a homoclinic orbit, which forms the boundary of a smaller safe basin. The ordinate of the homoclinic orbit is denoted as  $y_\delta(t)$ . The area of the safe basin can be obtained by integration as follows:

$$\begin{aligned} A_0 &= 2 \int_{x_1}^{x_2} y_0^+(t) dx_0(t) \\ &= 2 \int_{-\infty}^{\infty} [y_0^+(t)]^2 dt \end{aligned} \quad (3.5)$$

for the unbiased system, where  $x_1$  and  $x_2$  are the extrema of the roll angle of the safe basin, and

$$A_\delta = 2 \int_0^\infty y_\delta^2(t) dt \quad (3.6)$$

for the biased system, where  $t = 0$  is taken to be the point at which  $y_\delta = 0$  away from the saddle point.

Heteroclinic and homoclinic orbits are also known as separatrices, because they separate bounded and unbounded motions. The generalization of these boundaries to the damped forced ship motion is the key in analysing the global stability of this dynamical system. Figure 5 shows the ordinates of the separatrices for different heel angles, that is, for different levels of bias. It is noted that, by proper choice of the starting time,  $y_0^+(t)$  is an even function of  $t$  and  $y_\delta(t)$  is an odd function of  $t$ .

In the unperturbed system, i.e. the unforced and undamped system, the safe motions stay bounded forever. Under very small harmonic excitation and small damping, the motion generally remains periodic and bounded. As the excitation levels are increased, the motion becomes more complicated, even chaotic. Beyond a critical level of excitation, portions of the safe basin that are close to the unperturbed boundary may be transported out and become unbounded, resulting in capsizing (Thompson 1989*a,b*; Virgin 1987, 1989; Falzarano *et al.* 1992). For random excitations, transport between the safe and unsafe areas will always occur at some level of excitation,

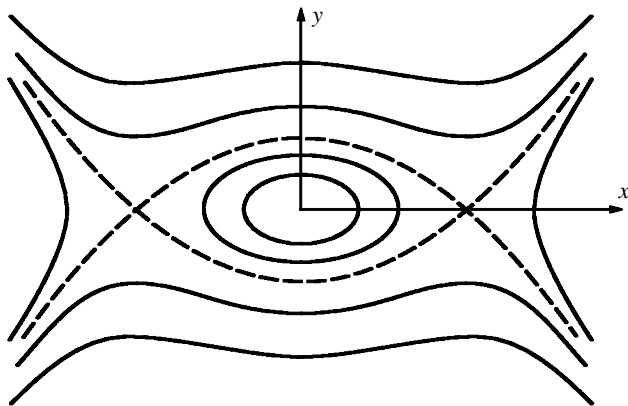


Figure 3. Phase plane for  $\delta = 0$ . Heteroclinic separatrix,  $\mathcal{W}_h$ , is shown as dashed lines. The two saddles are  $(-0.564, 0.0)$  and  $(+0.564, 0.0)$ .

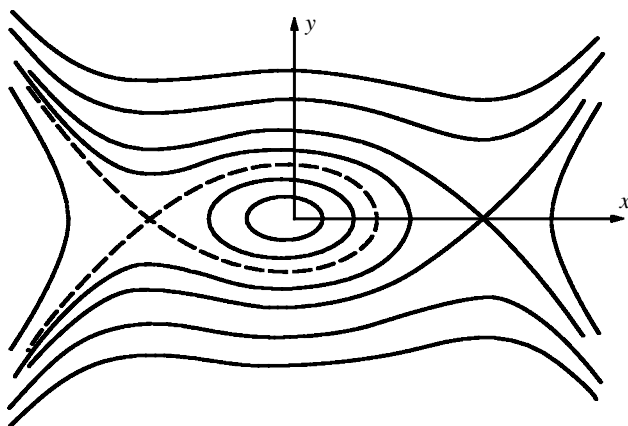


Figure 4. Phase plane for  $\delta = 0.070$ , equivalent to  $4^\circ$  heel angle. Homoclinic separatrix,  $\mathcal{W}_h$ , is shown as dashed lines. The two saddles are  $(-0.526, 0.0)$  and  $(+0.597, 0.0)$ .

but starts to become significant at a particular level of excitation amplitude (Hsieh *et al.* 1994). In this case, the rate of phase-space transport can be quantified by a well-defined Melnikov function (Hsieh *et al.* 1994).

### (b) The Melnikov function

Melnikov's method is a way to determine what happens to the separatrices associated with the system's saddle points when the damping and forcing effects are added to the unperturbed system. Roughly speaking, it is a measure of the separation of the stable and unstable manifolds of the saddle point. These are coincident in the unperturbed system, but this situation does not persist when excitation and damping are added. In particular, the separation can be expressed as a function of the excitation phase, specified by the initial time  $t_0$ , as  $d(t_0) = \epsilon M(t_0) + O(\epsilon^2)$ , where  $M(t_0)$  is the Melnikov function (Wiggins 1990). If the stable manifold, in the face of the perturbations, remains 'outside' of the unstable manifold for all time, the situation is stable

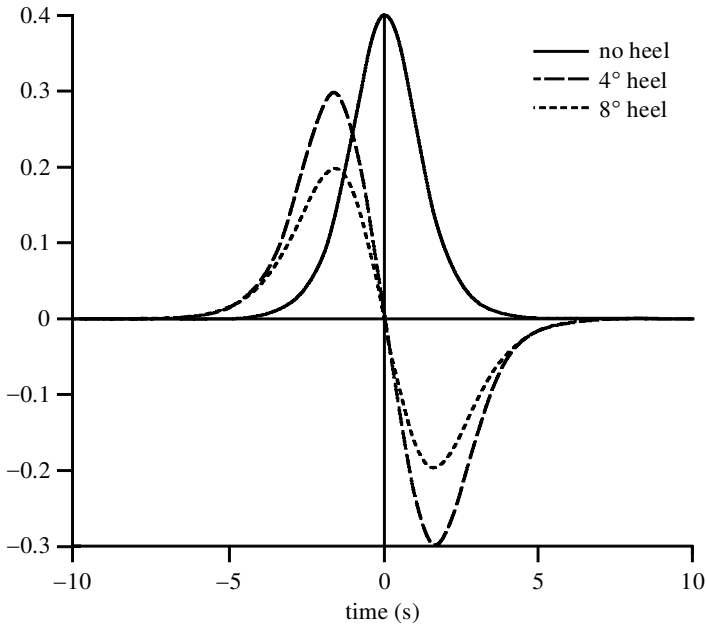


Figure 5. The ordinate of the separatrix  $y_0^+(t)$  for no heel,  $y_s(t)$  for biased cases.  $\delta = 0.070$  for  $4^\circ$  heel,  $\delta = 0.140$  for  $8^\circ$  heel.

in the sense that responses started inside the safe basin will remain stable, even if they are close to the basin boundary. In this case, the Melnikov function, by the sign convention generally adopted, will be negative for all time. On the other hand, if the stable manifold is ‘inside’ of the unstable manifold for all time, all solutions starting near the basin boundary will lead to capsize. Here, the Melnikov function is positive for all time. The more interesting case is when these manifolds cross one another as a function of time, continually switching relative orientations. (This is the situation when chaos appears (see Wiggins 1990).) In this case, some solutions started near the boundary will escape, and this opens the door for the possibility of capsize even if the vessel starts in the safe basin. In fact, chaotic transport theory shows that the area under the positive part of the Melnikov function is related to the rate at which solutions, as measured by volumes of the phase space, escape the safe basin. This is quantified by a measure of the time-averaged flux of phase space out of the safe basin—a quantity that is related directly to the Melnikov function, as described below.

Knowledge of this flux rate allows one to obtain a quantitative measure for the likelihood of capsize for a given vessel and sea state. Descriptions of this technique in the context of ship capsize can be found in the literature. The Melnikov theory for the usual roll differential equation has been considered in detail for both harmonic and random excitation (Falzarano *et al.* 1992, Hsieh *et al.* 1994; Jiang *et al.* 1996). However, the integro-differential equation requires special treatment. This is due to the fact that the integral term in the perturbation does not depend simply on the instantaneous values of the system states and time, but on the history of the roll velocity. This complicates the analysis and the interpretation of the perturbation in a non-trivial way. However, using a standard approach that approximates the memory

effects by the output of a finite-dimensional linear dynamical system, one can modify the Melnikov theory to handle these effects. The technical details of this analysis are presented in Appendix A. The net outcome of the results derived there is that one can procedurally treat the integral perturbation term in the usual manner that has been developed for perturbations of planar systems.

The Melnikov function associated with (3.1) and (3.2) is defined as (for details, see Hsieh *et al.* 1994; Jiang *et al.* 1996)

$$M_\delta(t_0) = \int_{-\infty}^{\infty} y_\delta(t) \left[ - \int_{-\infty}^{\infty} \delta_m(t-u)y_\delta(u) du - \delta_2 y_\delta(t) |y_\delta(t)| + f(t+t_0) \right] dt$$

$$= \tilde{M}_\delta(t_0) - \bar{M}_\delta, \tag{3.7}$$

where

$$\bar{M}_\delta = \int_{-\infty}^{\infty} y_\delta(t) \gamma_\delta(t) dt + \delta_2 \int_{-\infty}^{\infty} y_\delta(t)^2 |y_\delta(t)| dt, \tag{3.8}$$

$$\tilde{M}_\delta(t_0) = \int_{-\infty}^{\infty} y_\delta(t) f(t+t_0) dt \tag{3.9}$$

are the constant and oscillatory parts of the Melnikov function, respectively, and

$$\gamma_\delta(t, y) = \int_{-\infty}^{\infty} \delta_m(t-u)y_\delta(u) du. \tag{3.10}$$

For the unbiased case ( $\delta = 0$ ), the Melnikov function  $M_0(t_0)$  is defined along one of the heteroclinic orbits, in which case (Hsieh *et al.* 1994),

$$M_0(t_0) = \tilde{M}_0(t_0) - \bar{M}_0,$$

where

$$\bar{M}_0 = \int_{-\infty}^{\infty} y_0^+(t) \gamma_0(t, y) dt + \delta_2 \int_{-\infty}^{\infty} (y_0^+(t))^2 |y_0(t)| dt, \tag{3.11}$$

$$\tilde{M}_0(t_0) = \int_{-\infty}^{\infty} y_0^+(t) f(t+t_0) dt. \tag{3.12}$$

These results can be compared with those obtained from the standard differential equation model. Of course, the unperturbed versions of (2.9) and (2.10) are identical. And, even though the perturbed phase space is very different for these two cases, the corresponding Melnikov functions have similar form. In fact, the formulae of the oscillatory parts are the same (i.e. equations (3.9) and (3.12)), but the non-dimensional force  $f(t)$  is different from the dimensional excitation  $F(\tau)$ , simply because the total inertia used to scale  $\tau$  is different. Here, the constant part of the Melnikov function for (2.9) does not involve a memory term and is given by

$$\bar{M}_\delta = \delta_1 \int_{-\infty}^{\infty} y_\delta(t)^2 dt + \delta_2 \int_{-\infty}^{\infty} y_\delta(t)^2 |y_\delta(t)| dt. \tag{3.13}$$

In order to calculate  $\bar{M}_\delta$  in (3.8),  $\gamma_\delta(t, y)$  in (3.10) must first be determined. It is recognized from (3.10) that  $\gamma_\delta(t, y)$  is the convolution of  $K(t)$  and  $y_\delta(t)$ . It can be numerically evaluated by a combination of fast Fourier transform and the inverse

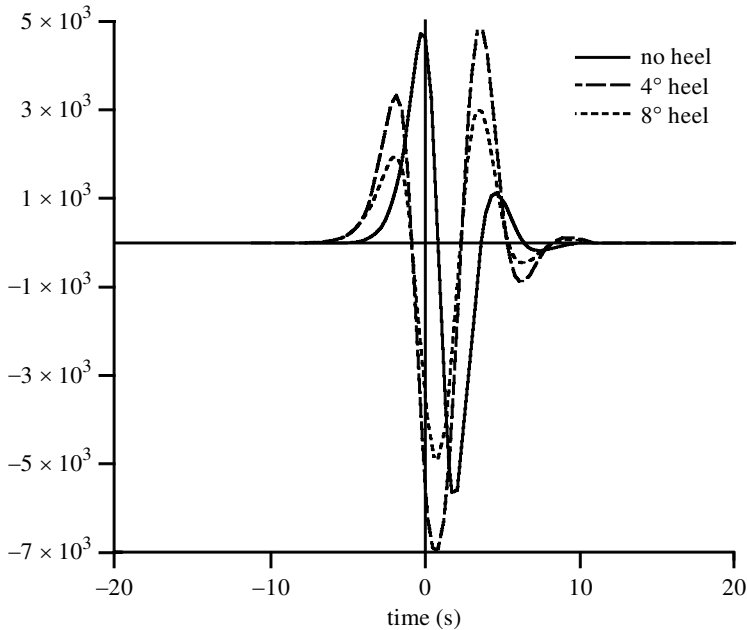


Figure 6. The intermediate function  $\gamma_\delta(t, y)$ .  $\delta = 0.070$  for  $4^\circ$  heel,  $\delta = 0.140$  for  $8^\circ$  heel.

fast Fourier transform (Bracewell 1978). The results for different values of the heel angle are presented in figure 6. Unlike the constant coefficient representation, where the linear damping  $\bar{M}_\delta$  changes proportionally with the linear damping coefficient (equation (3.13)), the memory-function representation of the linear hydrodynamic radiation influences  $\bar{M}_\delta$  in a complex manner through  $\gamma_\delta(t, y)$ . This will be explored further in §4.

(c) *Some features of the Melnikov function*

The constant part of the Melnikov function depends directly on the damping coefficients, while the oscillating part is linearly related to the excitation. The complete Melnikov function describes the relative orientation of the stable and unstable manifolds of the saddle point(s) at the angle(s) of vanishing stability as a function of time (via the forcing phase  $t_0$ ). For an unforced system with non-zero damping, the Melnikov function is a negative constant. This implies that the unstable manifolds of the saddle points at the angles of vanishing stability lie inside the corresponding stable manifolds (Guckenheimer & Holmes 1983; Wiggins 1990). In this case, all initial conditions located inside the safe basin of the associated undamped system will lead to motions that approach the stable upright position of the ship as  $t \rightarrow \infty$ . As the excitation amplitude is increased from zero, the Melnikov function starts to oscillate about its mean, with an amplitude proportional to the excitation level. When the forcing is sufficiently large that the Melnikov function crosses zero and is therefore positive for some duration of the excitation, the unstable manifold lies outside of the stable manifold, and solutions between them will be transported out of the safe region. These regions between the manifolds are known as ‘lobes’ (Wiggins 1992).

When lobes exist, the situation exists in which some solutions with initial conditions near the separatrix will escape to capsize.

For Gaussian excitation, the Melnikov function will have some zero crossings for any non-zero level of wave forcing, implying that there is a non-zero probability for capsizing as soon as the wave forcing is introduced. One consequence of this situation is that the dynamics of the system started near the boundary of the safe basin are essentially unpredictable, and capsize may occur (Thomson 1989*b*; Falzarano *et al.* 1992). In fact, for the case of harmonic excitation, the safe basin boundary has a fractal nature (Moon & Li 1985). In both the harmonic and random excitation cases, the likelihood of an initial condition escaping the safe region depends on a measure of the positive part of the Melnikov function. This can be quantified by knowing the mean frequency of the zero crossings of  $M(t_0)$ , the percentage of time that it is positive, and its positive amplitude. These, in turn, depend on the level of dissipation, through the mean value of  $M(t_0)$ , and on the overall amplitude and frequency content of the excitation, which dictate the oscillatory part of  $M(t_0)$ . Our goal here is to obtain a measure of these quantities and relate them to the likelihood of capsize.

(d) *The useful statistics of  $M(t_0)$*

For the case of random seas, the oscillatory part of the Melnikov function  $\tilde{M}_\delta(t_0)$  is a stochastic process. The results for this term are the same for both the differential and integro-differential system models, since damping affects only the mean value of  $M(t_0)$ . The correlation between  $\tilde{M}_\delta(t_0)$  and  $f(t)$  is linear, through the convolution integral indicated in (3.9) and (3.12). Using the evenness and oddness of the roll velocity taken along the basin boundaries, equations (3.9) and (3.12) can be transformed as follows:

$$\tilde{M}_\delta(t_0) = \int_{-\infty}^{\infty} -y_\delta(t_0 - t)f(t) dt \tag{3.14}$$

for the homoclinic case, and similarly for the heteroclinic case,

$$\tilde{M}_0(t_0) = \int_{-\infty}^{\infty} y_0^+(t_0 - t)f(t) dt. \tag{3.15}$$

If  $f(t)$  is a zero mean random process, then the expected value of  $\tilde{M}_0(t_0)$  is also zero,

$$E[\tilde{M}_\delta] = 0. \tag{3.16}$$

Under the assumption that  $f(t)$  is stationary, the spectrum of  $\tilde{M}_\delta(t_0)$  is given by

$$S_{\tilde{M}_\delta}^+(\Omega) = (2\pi)^2 |Y_\delta(\Omega)|^2 S_f^+(\Omega) \tag{3.17}$$

$$= (2\pi)^2 |Y_\delta(\Omega)|^2 |F_{\text{roll}}(\Omega)|^2 S_\zeta^+(\Omega), \tag{3.18}$$

where  $Y_\delta(\Omega)$  is the Fourier transform of  $y_\delta(t)$ ,

$$Y_\delta(\Omega) = \frac{1}{2\pi} \int_{-\infty}^{\infty} y_\delta(t)e^{-i\Omega t} dt, \tag{3.19}$$

and  $S_f^+(\Omega)$ ,  $F_{\text{roll}}(\Omega)$  and  $S_\zeta^+(\Omega)$  are the scaled forcing spectrum, roll moment per unit wave height and incident wave spectrum, respectively.

The Gaussian and ergodic natures of a random process are preserved under linear transformations. Thus, if the random wave elevation  $\zeta(t)$  is a stationary ergodic Gaussian random process, then the roll excitation  $f(t)$  and the oscillatory part of Melnikov function  $\tilde{M}_\delta(t_0)$  will share those properties, since they are all linearly related to one another. For this stationary random process, the mean square value, the autocorrelation function and the power spectrum are related as follows:

$$\begin{aligned} R_{\tilde{M}_\delta}(s, t) &= R_{\tilde{M}_\delta}(s - t) \\ &= R_{\tilde{M}_\delta}(\tau) \\ &= \int_0^\infty S_{\tilde{M}_\delta}^+(\Omega) e^{-i\Omega\tau} d\Omega, \end{aligned} \tag{3.20}$$

$$\begin{aligned} E[\tilde{M}_\delta^2(t_0)] &= R_{\tilde{M}_\delta}(0) \\ &= \int_0^\infty S_{\tilde{M}_\delta}^+(\Omega) d\Omega, \end{aligned} \tag{3.21}$$

where  $\tau = s - t$  and  $R_{\tilde{M}_\delta}(s, t)$  is a function of  $\tau$  only because  $\tilde{M}_\delta(t_0)$  is stationary. By using (3.18), (3.16), (3.17) and (3.21), one can obtain the following relationship between the variance of  $\tilde{M}_\delta(t_0)$  and the spectrum of the wave elevation:

$$\begin{aligned} \sigma_{\tilde{M}_\delta}^2 &= E[\tilde{M}_\delta^2(t_0)] \\ &= \int_0^\infty (2\pi)^2 |Y_\delta(\Omega)|^2 |F_{\text{roll}}(\Omega)|^2 S_\zeta^+(\Omega) d\Omega. \end{aligned} \tag{3.22}$$

Because  $\tilde{M}_\delta(t_0)$  is a stationary Gaussian process, it is uniquely determined by its mean  $\tilde{M}_\delta$  and variance  $\sigma_{\tilde{M}_\delta}^2$ . The zero-mean random variable  $x = \tilde{M}_\delta(t_0)$  has the following probability density function at any value of  $t_0$ :

$$p_{\tilde{M}_\delta}(x) = \frac{1}{\sqrt{2\pi}\sigma_{\tilde{M}_\delta}} \exp\left(-\frac{x^2}{2\sigma_{\tilde{M}_\delta}^2}\right). \tag{3.23}$$

This Gaussian structure will yield an analytical measure for the positive part of the Melnikov function.

*(e) Phase-space transport and the Melnikov function*

The amount of phase space transported out of the safe region is related to the areas of the lobes formed when the stable manifold is inside of the unstable manifold, i.e. where  $M(t_0) > 0$ . (Recall that these are the situations for which solutions can escape the safe region.) This area can be approximated in asymptotic form by integrating the Melnikov function over those times for which it is positive (Wiggins 1992). For a random process, the following sum of integrals of the Melnikov function provides the desired measure of the area of phase space transported out of the safe region over a given time interval (Frey & Simiu 1993):

$$\mu = \epsilon \sum_i \int_{t_{i1}}^{t_{i2}} M_\delta(t_0) dt_0 + O(\epsilon^2), \tag{3.24}$$

where  $[t_{i1}, t_{i2}]$  is the  $i$ th interval over which  $M_\delta(t_0) > 0$ .

In order to have a more useful measure of the likelihood of the escape of solutions out of the safe basin under random excitation, we take the long-time average of this quantity, resulting in a rate of phase-space flux, as follows (Hsieh *et al.* 1994):

$$\begin{aligned}\Phi_\delta &= \lim_{T \rightarrow \infty} \frac{\epsilon}{2T} \int_{-T}^T M_\delta^+(t_0) dt_0 + O(\epsilon^2) \\ &= \lim_{T \rightarrow \infty} \frac{\epsilon}{2T} \int_{-T}^T (\tilde{M}_\delta(t_0) - \bar{M}_\delta)^+ dt_0 + O(\epsilon^2),\end{aligned}\quad (3.25)$$

where  $M_\delta^+(t_0)$  denotes the positive part of the Melnikov function. Since  $M_\delta(t_0)$  is an ergodic stationary Gaussian process, the time average of  $M_\delta(t_0)$  is equal to its ensemble average,

$$\begin{aligned}\lim_{T \rightarrow \infty} \frac{1}{2T} \int_{-T}^T M_\delta^+(t_0) dt_0 &= E[M_\delta^+(t_0)] \\ &= E[(\tilde{M}_\delta(t_0) - \bar{M}_\delta)^+].\end{aligned}$$

Therefore, the rate of phase-space flux becomes, to leading order,

$$\Phi_\delta = \epsilon E[(\tilde{M}_\delta(t_0) - \bar{M}_\delta)^+] + O(\epsilon^2) \quad (3.26)$$

$$= \epsilon \int_{\bar{M}_\delta}^{\infty} (x - \bar{M}_\delta) p_{\tilde{M}_\delta}(x) dx + O(\epsilon^2), \quad (3.27)$$

where  $x$  is a random variable representing the Gaussian random process  $\tilde{M}_\delta(t_0)$ , with zero mean, variance  $\sigma_{\tilde{M}_\delta}^2$  and the PDF given in (3.23).

The standard Gaussian probability density function  $p(z)$  and the associated probability distribution function  $P(z)$  are related as follows:

$$p(z) = \frac{1}{\sqrt{2\pi}} \exp\left(-\frac{1}{2}z^2\right), \quad (3.28)$$

$$P(z) = \int_{-\infty}^z p(x) dx. \quad (3.29)$$

Using these relationships, equation (3.27) can be written as

$$\begin{aligned}\Phi_\delta &= \epsilon \int_{\bar{M}_\delta}^{\infty} (x - \bar{M}_\delta) \frac{1}{\sqrt{2\pi}\sigma_{\tilde{M}_\delta}} \exp\left(-\frac{x^2}{2\sigma_{\tilde{M}_\delta}^2}\right) dx + O(\epsilon^2) \\ &= \epsilon \sigma_{\tilde{M}_\delta} \int_{\bar{M}_\delta/\sigma_{\tilde{M}_\delta}}^{\infty} \frac{1}{\sqrt{2\pi}} \left(z - \frac{\bar{M}_\delta}{\sigma_{\tilde{M}_\delta}}\right) \exp\left(-\frac{1}{2}z^2\right) dz + O(\epsilon^2) \\ &= \epsilon \left[ \sigma_{\tilde{M}_\delta} p\left(\frac{\bar{M}_\delta}{\sigma_{\tilde{M}_\delta}}\right) + \bar{M}_\delta P\left(\frac{\bar{M}_\delta}{\sigma_{\tilde{M}_\delta}}\right) - \bar{M}_\delta \right] + O(\epsilon^2)\end{aligned}\quad (3.30)$$

for the biased case, and as

$$\Phi_{\text{upper}} = \epsilon \left[ \sigma_{\tilde{M}_0} p\left(\frac{\bar{M}_0}{\sigma_{\tilde{M}_0}}\right) + \bar{M}_0 P\left(\frac{\bar{M}_0}{\sigma_{\tilde{M}_0}}\right) - \bar{M}_0 \right] + O(\epsilon^2) \quad (3.31)$$

for the unbiased case. Here,  $\Phi_{\text{upper}}$  is the rate of phase-space flux through the upper heteroclinic orbit.

If we denote  $\sigma_\delta^1$  as the RMS value of  $\tilde{M}_\delta(t_0)$  for unit significant wave height, and note that  $\sigma_{\tilde{M}_\delta}$  is proportional to the significant wave height  $H_s$ ,  $\Phi_\delta$  can be rewritten in a form normalized by the area of the unperturbed safe basin, as follows:

$$\frac{\Phi_\delta}{A_\delta} = \frac{\epsilon}{A_\delta} \left[ H_s \sigma_\delta^1 p \left( \frac{\bar{M}_\delta}{H_s \sigma_\delta^1} \right) + \bar{M}_\delta P \left( \frac{\bar{M}_\delta}{H_s \sigma_\delta^1} \right) - \bar{M}_\delta \right] + O(\epsilon^2). \quad (3.32)$$

The dependence of the flux rate  $\Phi_\delta/A_\delta$  in (2.10) on the significant wave height  $H_s$  for several values of bias, at a characteristic wave period  $T_s = 9.0$  s, is shown in figure 7. Note that there is a finite amount of phase-space flux for any non-zero excitation. This means that there is a finite probability of capsizing for any non-zero wave height, although for small wave heights, capsizing is highly unlikely over any reasonable exposure time. The flux rate is very small for small wave heights, but begins to grow significantly beyond a critical wave height, after which it grows steadily as  $H_s$  increases, eventually approaching a linear asymptote. This asymptote is achieved as  $H_s \rightarrow \infty$ , and is given by

$$\frac{\Phi_\delta}{A_\delta} \approx \frac{\epsilon}{A_\delta} \left( \frac{1}{\sqrt{2\pi}} H_s \sigma_\delta^1 - \frac{1}{2} \bar{M}_\delta \right). \quad (3.33)$$

The asymptote, shown in figure 7 for three values of the heel angle, intersects the  $H_s$ -axis at a wave height given by

$$H_s^* = \frac{\sqrt{2\pi} \bar{M}_\delta}{2\sigma_\delta^1}. \quad (3.34)$$

We define  $H_s^*$  as the critical wave height at which substantial phase-space flux begins to occur, suggesting an increased risk of operating the ship. It provides a measure of the combined effects of the large-amplitude roll characteristics of the vessel, the amount of dissipation present and the nature of the wave excitation in a relatively simple way. Figure 8 shows how  $H_s^*$  varies with the characteristic wave period and the heel angle.

As pointed out by Hsieh *et al.* (1994), the exact quantitative relation of the rate of phase-space flux  $\Phi_\delta$  and the likelihood of capsizing depends on the distribution of the response in the phase space, the location of the phase space being transported, the replenishing of phase space into the safe basin from the unsafe area and the exposure time. The details of such relationships are presently unknown. However, simulation results presented by Hsieh *et al.* (1994) demonstrated a high correlation between  $\Phi_\delta$  and the probability of capsizing. We use  $H_s^*$  as the critical significant wave height because, graphically, it represents the starting point where the rate of phase-space flux increases virtually linearly with the significant wave height.

If one deems that  $H_s^*$  corresponds to a capsizing probability too high (or too low) to be acceptable, one can calculate a different criterion. For example, one can define a certain rate of phase-space flux, and compute the associated significant wave height for different characteristic wave periods, using (3.32). Critical wave height curves computed in this manner take similar shapes to the shape of the  $H_s^*$  curve. However, they differ since the  $H_s^*$  curve does not maintain a constant rate of phase-space flux as the wave period varies. The results for the *Patti-B* are shown in figures 9, 10 and 11 for a 0, 4 and 8° bias angle, respectively. Also note that the rates of phase-space flux at  $H_s^*$  change significantly with the bias angle. In the unbiased case, the rate of phase-space flux at  $H_s^*$  is approximately 0.004, while it is about 0.0035 and 0.0025 for the 4 and 8° bias cases, respectively.

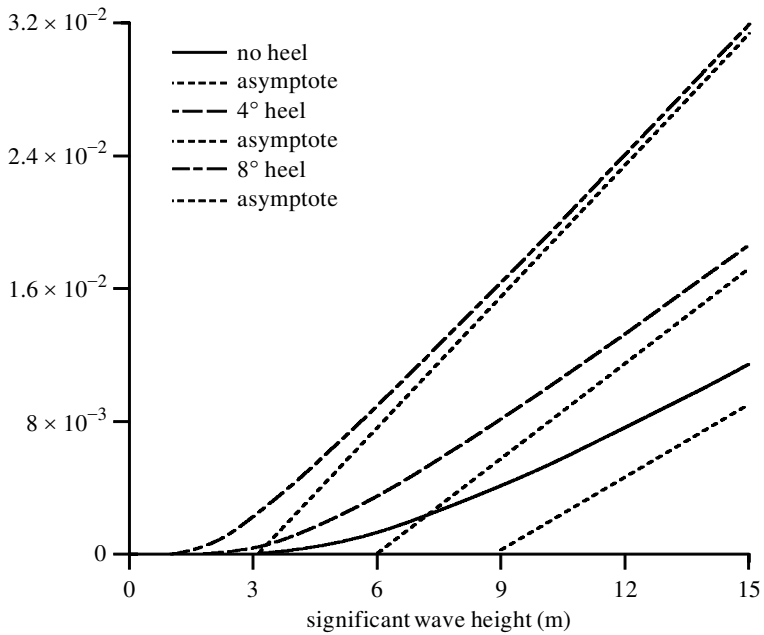


Figure 7. The rate of phase-space flux at 9.0 s characteristic wave period considering memory effects,  $2\Phi_{\text{upper}}/A_0$  for the zero heel and  $\Phi_\delta/A_\delta$  for the rest. The short broken lines are the linear asymptotes.

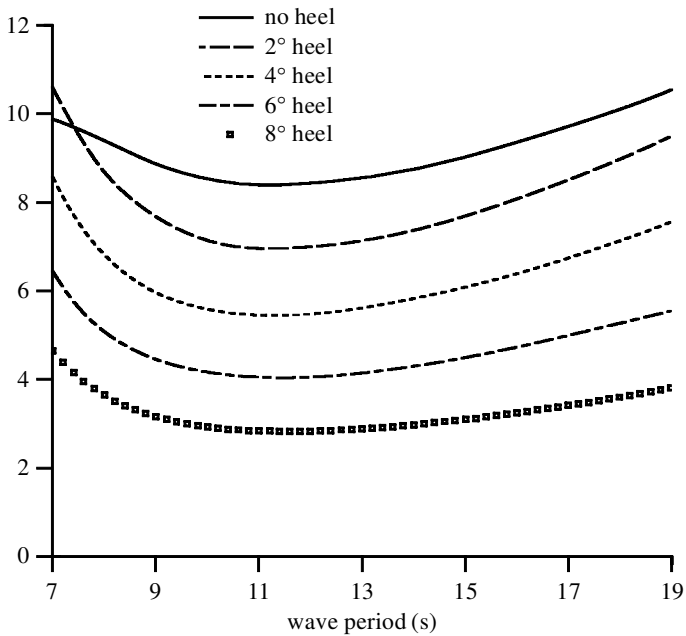


Figure 8. The critical significant wave height  $H_s^*$ . Memory effects are taken into account.

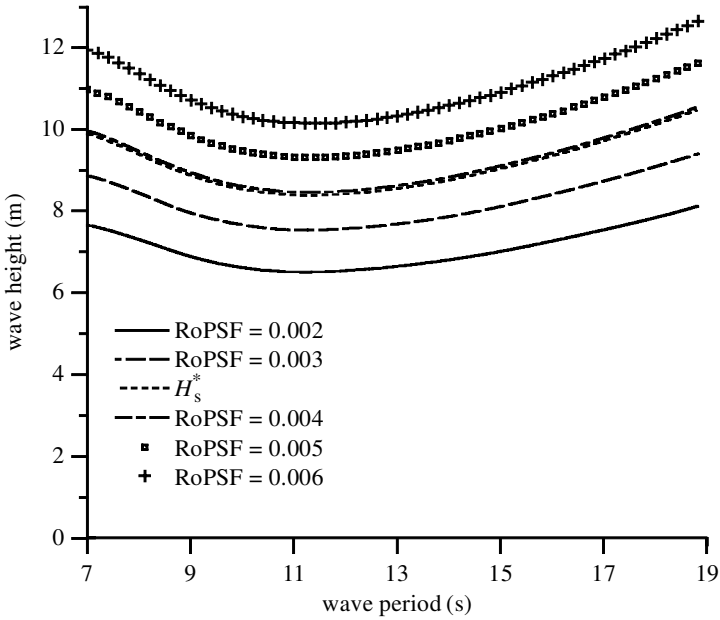


Figure 9. The significant wave height at 0° heel corresponding to equal level of phase-space flux compared with the critical significant wave height  $H_s^*$ . ‘RoPSF’ refers to the rate of phase-space flux.

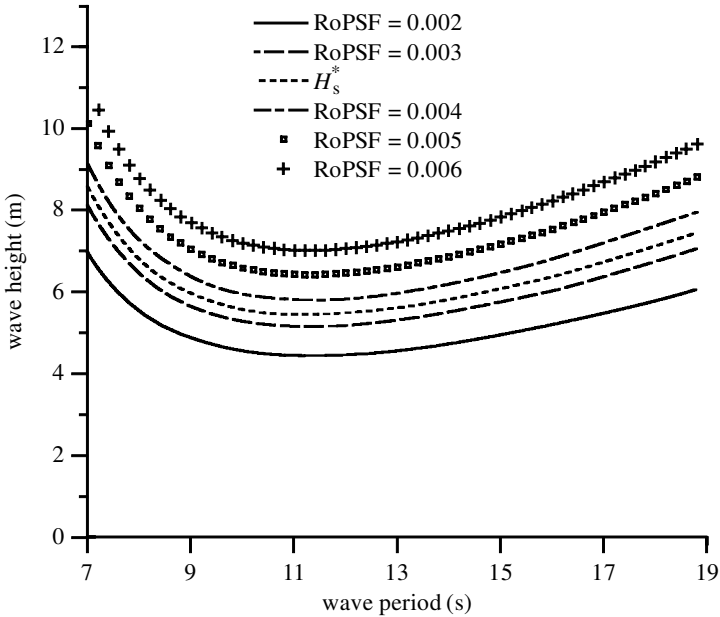


Figure 10. The significant wave height at 4° heel corresponding to equal level of phase-space flux compared with the critical significant wave height  $H_s^*$ . ‘RoPSF’ refers to the rate of phase-space flux.

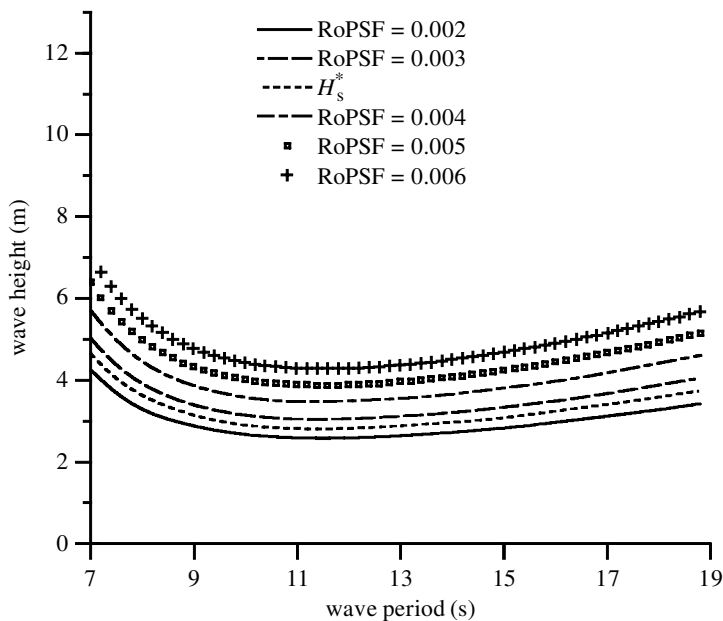


Figure 11. The significant wave height at  $8^\circ$  heel corresponding to equal level of phase-space flux compared with the critical significant wave height  $H_s^*$ . ‘RoPSF’ refers to the rate of phase-space flux.

#### 4. The effects of the damping model on the critical wave height

Similar calculations for  $H_s^*$  have been previously carried out for the system with the usual linear and quadratic damping terms, i.e. equation (2.9) (Jiang *et al.* 1996). However, as mentioned before, there is some uncertainty in the linear damping coefficient when these constant coefficient models are employed, since no single frequency is present in the response. The range of possible values includes those at the linear natural roll frequency  $\omega_n$ , or a typical excitation frequency, such as the characteristic wave frequency  $\omega_z$ , but neither are the correct representation. Using the memory-dependent model, one can determine the importance of the linear damping model employed, and the effect that various approximations and assumptions will have on the prediction of system behaviour in terms of capsize probability. These results can be used to determine the most appropriate value of the frequency for evaluating the equivalent linear damping coefficient in the constant coefficient models.

To investigate these issues, we calculated  $H_s^*$  for three cases of constant frequency:  $B_{44} = 0.0$ ,  $B_{44} = B_{44}(\omega_n)$  and  $B_{44} = B_{44}(\omega_z)$ , and the results were compared with those from the memory function model. The results are depicted in figures 12, 13 and 14 for heel angles of  $0^\circ$ ,  $4^\circ$  and  $8^\circ$ , respectively. The linear damping model, which uses the memory function, accounts for 16% of the total damping effect in the unbiased case, as shown in table 2. That is, the difference between  $H_s^*$  with the memory function and  $H_s^*$  with no linear damping is 16% of the final  $H_s^*$  value. The influence of the memory function model is increased in the biased systems, to 27% for  $4^\circ$  heel, and to 34% for  $8^\circ$  heel. Similar conclusions are found to hold for the model that assumes  $B_{44} = B_{44}(\omega_n)$ , where it represents 15, 18 and 26% of the total damping for  $0^\circ$ ,  $4^\circ$  and  $8^\circ$  heel angles, respectively. Similarly, for the model that assumes  $B_{44} = B_{44}(\omega_z)$ ,

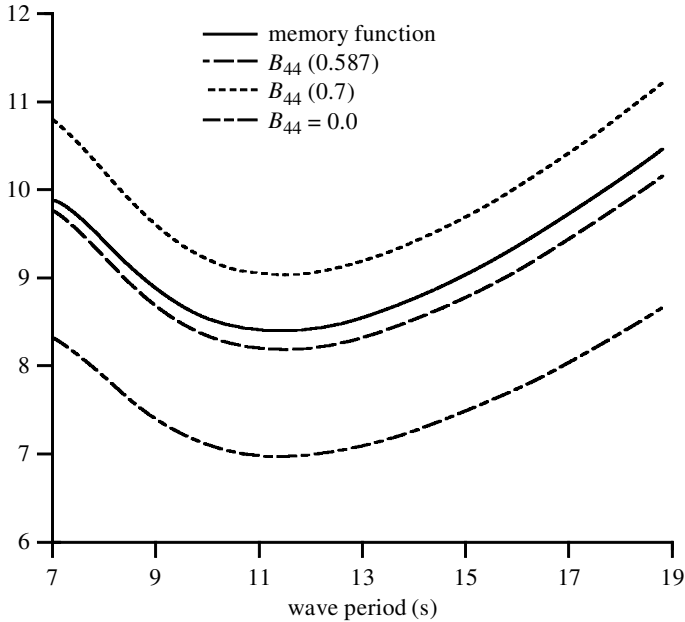


Figure 12. The influence of linear damping modelling on the critical significant wave height  $H_s^*$  in zero heel.  $B_{44}(0.587)$  corresponds to  $\omega = \omega_n$ .  $B_{44}(0.700)$  corresponds to a typical excitation frequency  $\omega = 0.700$ .

the results are 23, 28 and 37% for 0, 4 and 8° heel angles, respectively. It is seen that, for the vessel under consideration, the model using  $B_{44} = B_{44}(\omega_n)$  underestimates the effects of linear damping, leading to conservative safety predictions. On the other hand, the  $B_{44} = B_{44}(\omega_z)$  model slightly overestimates the damping effect, resulting in an underestimation of the actual likelihood of capsizing. There is no reason to expect that these trends will be universal. If the constant coefficient model is to be used for ship stability studies, the ‘best’ value for  $B_{44}$  will depend on the ship’s natural frequency, the ship geometry and the characteristics of the wave spectrum.

The  $B_{44} = B_{44}(\omega_n)$  model can approximately achieve the same damping effect as the memory function model and causes only small error in  $H_s^*$  in the unbiased case (see figure 12). However, when the vessel heels, the  $B_{44} = B_{44}(\omega_n)$  model underestimates  $H_s^*$ . In contrast, the  $B_{44} = B_{44}(\omega_z)$  model overestimates  $H_s^*$  for the unbiased system (it yields almost double the actual linear damping effect), but closely matches the memory function result for the two biased cases considered. It is anticipated that, for other heel angles,  $B_{44}$  at other frequencies would offer better estimates for  $H_s^*$ . It must be concluded that, in general, there is no ‘best’ frequency.

## 5. Simulations of the integro-differential equations

### (a) The simulation model

In this section, time-domain simulation is used to calibrate the capsizing probability at the critical significant wave height  $H_s^*$ . Random time histories (realizations) of the roll moment are generated from the spectrum (equation (2.2)) by the scheme proposed by Cuong *et al.* (1982). The equations of motion for the different models

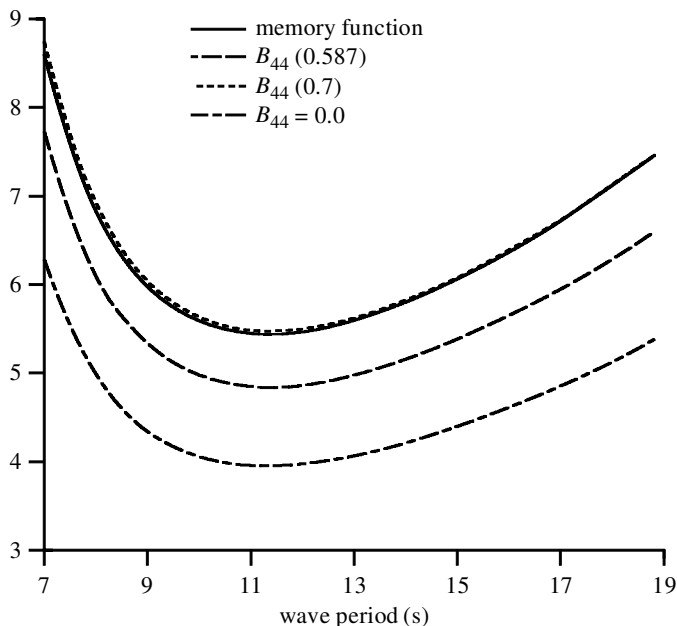


Figure 13. The influence of linear damping modelling on the critical significant wave height  $H_s^*$  in  $4^\circ$  heel.  $B_{44}(0.587)$  corresponds to  $\omega = \omega_n$ .  $B_{44}(0.700)$  corresponds to a typical excitation frequency  $\omega = 0.700$ .

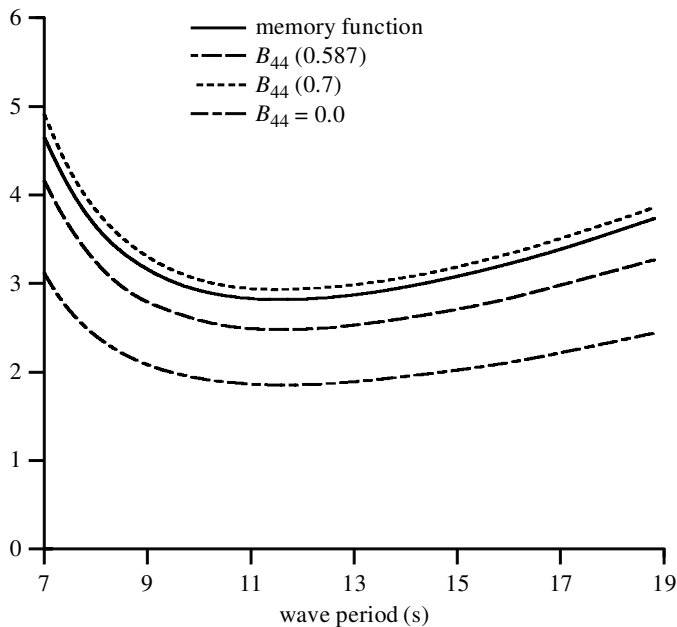


Figure 14. The influence of linear damping modelling on the critical significant wave height  $H_s^*$  in  $8^\circ$  heel.  $B_{44}(0.587)$  corresponds to  $\omega = \omega_n$ .  $B_{44}(0.700)$  corresponds to a typical excitation frequency  $\omega = \omega_z = 0.700$ .

Table 2. *The asymptotic significant wave heights for different linear damping models*

(The characteristic wave period is 9.0 s for all cases.  $B_{44}(\omega_n) = 0.321 \times 10^4 \text{ kg m}^{-2} \text{ s}^{-1}$ ,  $B_{44}(\omega_z) = 0.548 \times 10^4 \text{ kg m}^{-2} \text{ s}^{-1}$ ,  $\omega_n = 0.587 \text{ rad s}^{-1}$ ,  $\omega_z = 0.700 \text{ rad s}^{-1}$ .)

| $T_s = 9.0 \text{ s}$       | 0° heel | 4° heel | 8° heel |
|-----------------------------|---------|---------|---------|
| damping modelling (m)       | $H_s^*$ | $H_s^*$ | $H_s^*$ |
| memory function             | 8.87    | 5.97    | 3.15    |
| $B_{44} = B_{44}(\omega_n)$ | 8.68    | 5.33    | 2.79    |
| $B_{44} = B_{44}(\omega_z)$ | 9.59    | 6.03    | 3.29    |
| $B_{44} = 0.0$              | 7.40    | 4.35    | 2.07    |

are then integrated for an exposure time of up to 34.1 min. Capsize is defined as the roll angle exceeding the angle of vanishing stability at any time during the exposure period. For each significant wave height and characteristic wave period combination, 500 realizations are used. Each realization is based on a statistically equivalent but temporally different roll-excitation time history. The initial roll angle and roll velocity are set equal to zero.

For the usual roll differential equation, i.e. equation (2.1), there are no special numerical difficulties. However, integration of the history-dependent integro-differential system is not so straightforward, due to the convolution integral. There exist several methods in the literature to numerically integrate the integro-differential equation, i.e. equations (2.4) or (2.8), depending how the convolution integral is handled.

The direct integration method is used by Takagi *et al.* (1984) in their study of motions of moored bodies. This is effective since the impulse response function is non-zero over a relatively short period (figure 2) and direct integration of the convolution integral is quick. If the memory effects span a large time interval, this method becomes inefficient.

Another approach to this class of systems is to use an augmented state space (see, for example, McCreight 1986; Jiang *et al.* 1987; Holappa & Falzarano 1999). Such an approach is often quite useful, and in this study it provides a relatively simple means of justifying the application of the planar Melnikov method (see appendices A and B). This method uses an augmented state space to approximate the convolution integral by a system of  $n$  linear ODEs whose transfer function can be constructed from the linear damping and added mass coefficients in a systematic, but not unique, manner (Warwick 1989). In this way, evaluation of the convolution integral is avoided at the expense of expanding the original system of two ODEs into  $n + 2$  first-order ODEs. However, the new  $n + 2$  equations are only an approximation of the real system, hopefully converging with large  $n$ . Such a procedure is described in detail in Appendix B.

In this work, we use direct integration, since the system memory is *ca.* 8 s (figure 2). The computation time of solving the integro-differential equations in this manner is approximately only twice that of using the constant coefficient equations, i.e. equation (2.8). For direct simulation, a fourth-order Runge–Kutta method is employed. Errors may arise from the usual round-off and from the truncation of the memory function. The usual round-off errors are dealt with by choosing an appropriate step size, which was found to be about 150 time-steps per characteristic wave period. Sample simulation results show that the length of the memory function is not of

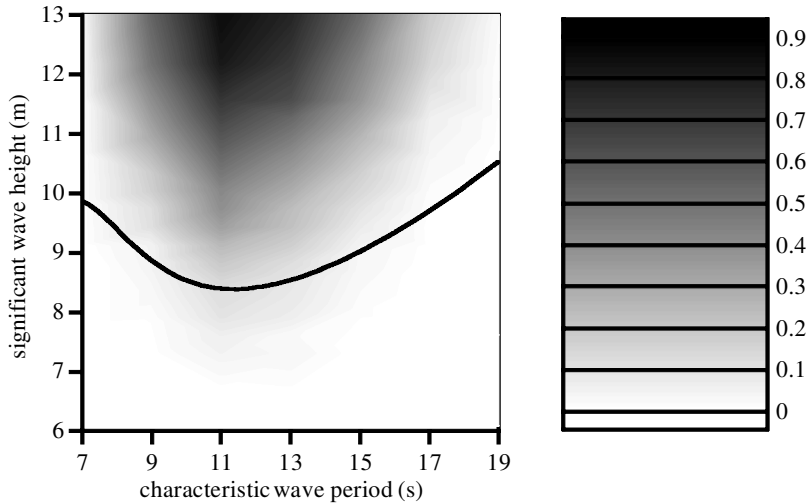


Figure 15. Comparison between simulation and theoretical results for  $0^\circ$  heel angle with memory effect being accounted for. The integration time-step is 0.0625 s.

primary importance in estimating the probability of capsize, provided that its most significant part, i.e. the first 8 s, is not discarded (Jiang 1995).

#### (b) *The results of simulation*

The results of simulations, including memory effects, are summarized in figures 15, 16 and 17, which show a comparison of capsize probability with the prediction of Melnikov analysis. The probability of capsize around the critical significant wave height curve is in the range of 3–7, 5–9 and 1–4% for the unbiased,  $-4^\circ$  heel and  $-8^\circ$  heel cases, respectively. As can be seen from these figures, the theoretical asymptote qualitatively matches the results of the simulations quite well. The likelihood of capsize, as predicted by the theoretical critical curves, varies from the simulation results by 1–9% for the heel angles and exposure times under consideration. However, the relative ease of computing this curve, when compared against the extensive nature of the stochastic simulations, strongly recommends its use as an investigative engineering tool.

## 6. Conclusions

On a general level, this work has shown that analysis tools from the theory of dynamical systems can be used to examine nonlinear systems with memory and random excitation. The applications of the Melnikov function and phase-space transport techniques are used to predict extreme responses that lead to failure. The methodology is quite general and can be applied to expanded multi-degree-of-freedom systems. There are no restrictions on the nature of the memory function, other than it needs to be modelled by a linear integro-differential equation, or an expanded state space model.

In this work, these methods have been applied to the capsizing of ships in a random seaway. Closed-form asymptotic expressions for the rate of phase-space flux and

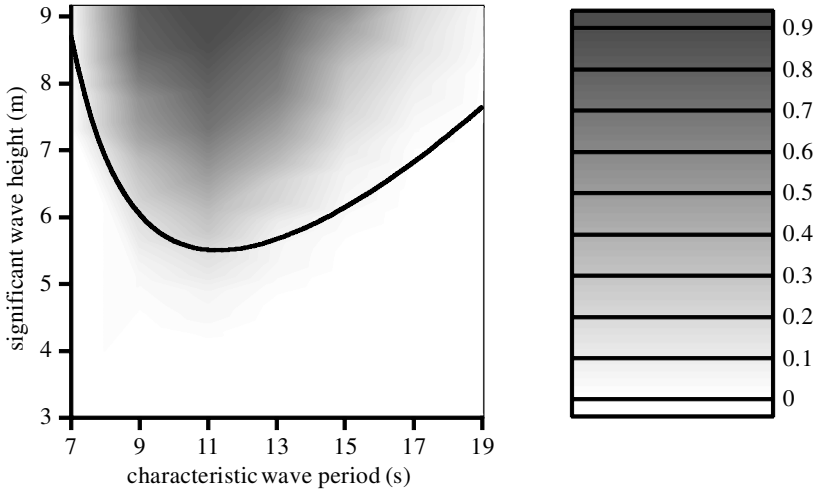


Figure 16. Comparison between simulation and theoretical results for  $-4^\circ$  heel angle with memory effect being accounted for. The integration time-step is 0.0625 s.

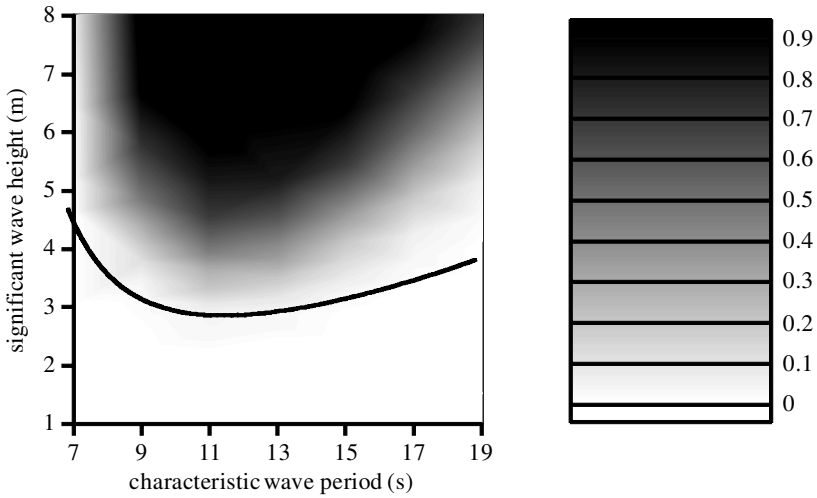


Figure 17. Comparison between simulation and theoretical results for  $-8^\circ$  heel angle with memory effect being accounted for. The integration time-step is 0.0625 s.

an associated critical significant wave height are derived and evaluated using simulations. Using these results, it was found that the memory function influences the probability of capsize. And, while one can replace the memory function with constant added mass and damping coefficients evaluated at a single frequency, a general relation for the determination of the ‘best’ frequency could not be found. Depending upon vessel conditions (heel angle and mass distribution) and sea environment (significant wave height and characteristic wave period), different strategies for the selection of the ‘best’ frequency may be possible. It is expected that none of these strategies is universal. As such, it is recommended that the hydrodynamic coefficients include the influence of memory effects.

This paper has been sponsored by the Michigan Sea Grant College Program, Projects R/T-32 and R/T-37, under grant numbers NA89AA-D-SG083 Amd#5 and DOC-G-NA76RG0133 from the Office of Sea Grant, National Oceanic and Atmospheric Administration (NOAA), US Department of Commerce, and funds from the State of Michigan. The government is authorized to produce and distribute reprints for government purpose notwithstanding any copyright notation appearing herein. S.W.S. also acknowledges partial support from the National Science Foundation and helpful discussions with Hassan Khalil on linear system dynamics.

## Appendix A. The Melnikov function for systems with memory effects

In this appendix we provide the technical justification for the Melnikov function used in the paper, and for the use of phase-space transport ideas for this class of systems. This is necessary because the perturbation terms in the integro-differential equation are not simply dependent on the instantaneous states of the system and the forcing phase; they also depend on the history of the states. Therefore, the perturbed phase space is actually infinite dimensional. In this derivation, we will use an expanded state space model to approximate the memory effects. We begin by approximating the memory term as the output of a finite-dimensional dynamical system. The procedure for accomplishing this is described in detail in Appendix B. We then use the general structure of these systems to derive the appropriate Melnikov function and provide an interpretation of the phase-space transport. The key step to the approach taken is to show that the dynamics of this high-dimensional system really take place in a low-dimensional stable invariant manifold, on which the usual results apply.

The memory term can be approximated by the output of some finite-dimensional linear system, as follows. First, denote

$$z_1(y, t) = \int_{-\infty}^{\infty} \delta_m(t - u)y(u) du \quad (\text{A } 1)$$

and let  $z_1(y, t)$  be the first element of a vector  $\mathbf{z}(y, t)$ , whose dynamics are governed by a linear system of the form

$$\dot{\mathbf{z}} = \mathbf{A}\mathbf{z} + \mathbf{b}y, \quad (\text{A } 2)$$

where the (scalar) roll velocity  $y$  plays the role of an input. In this setting, the equations of motion, in first-order form, are given by

$$\begin{aligned} \dot{x}(t) &= y(t), \\ \dot{y}(t) &= f(x) + \epsilon g(x, y, \mathbf{c}\mathbf{z}, t), \\ \dot{\mathbf{z}} &= \mathbf{A}\mathbf{z} + \mathbf{b}y, \end{aligned}$$

where the specific forms of  $f(x)$ ,  $g(x, y, \mathbf{c}\mathbf{z}, t)$ ,  $\mathbf{A}$  and  $\mathbf{b}$  can be found by comparison with the equations given in Appendix B, and  $\mathbf{c}$  is simply a vector that picks off the first element of  $\mathbf{z}$ . Our goal here is to show that the first two equations correctly capture the full dynamics, at least in some invariant manifold of the  $(x, y, \mathbf{z})$  phase space, by replacing  $\mathbf{z}$  with an appropriate function of  $(x, y)$  on the invariant manifold. In that case, the usual Melnikov theory goes through, as does the interpretation of phase-space transport for periodically forced oscillators (Wiggins 1992).

In the unperturbed system (i.e.  $\epsilon = 0$ ), the  $(x, y)$  dynamics are uncoupled from the  $\mathbf{z}$  dynamics. For notational purposes, we denote the unperturbed solutions as

$(x, y, z) = (x_\delta, y_\delta, z_\delta)$ . As described in §5, the  $(x_\delta, y_\delta)$  dynamics are those of the well-known conservative phase planes shown in figures 3 and 4. Once  $y_\delta$  is known from the  $(x_\delta, y_\delta)$  system, the  $z_\delta$  dynamics are those of a linear system with known input. The specific solution of interest here is the one that is bounded for all time when the input  $y$  is bounded and the eigenvalues of  $\mathbf{A}$  are all stable; it is given by

$$z_\delta(y, t) = \int_{-\infty}^t e^{\mathbf{A}(t-\tau)} \mathbf{b} y_\delta(\tau) \, d\tau. \tag{A 3}$$

These solutions for  $\mathbf{z}$  represent, in the fully extended  $(x, y, z)$  phase space, a two-dimensional invariant manifold of the form  $\mathbf{z} = \mathbf{F}_0(x, y)$ . Furthermore, since the transient part of the  $\mathbf{z}$  dynamics is exponentially stable, this is an attracting manifold.

For  $0 < \epsilon \ll 1$ , the  $(x, y, z)$  dynamics become fully coupled. For this system, there exists an asymptotically stable, perturbed manifold of the form  $\mathbf{F} = \mathbf{F}_0 + \epsilon \mathbf{F}_1 + \dots$ . On this manifold, the equations of motion are given by

$$\left. \begin{aligned} \dot{x}(t) &= y(t), \\ \dot{y}(t) &= f(x) + \epsilon g(x, y, \mathbf{c}\mathbf{F}_0(x, y), t) + O(\epsilon^2). \end{aligned} \right\} \tag{A 4}$$

The Melnikov function for this two-dimensional system is then given by the usual planar result, as follows:

$$M_\delta(t_0) = \int_{-\infty}^{\infty} y_\delta(t) g(x_\delta, y_\delta, \mathbf{c}\mathbf{z}_\delta, t + t_0) \, dt, \tag{A 5}$$

where the unperturbed solution is taken along the homoclinic or heteroclinic orbit.

Finally, by identifying the various terms and their roles in the perturbation function  $g$ , especially the fact that

$$\mathbf{c}\mathbf{z} = z_1 = \int_{-\infty}^{\infty} \delta_m(t - u) y(u) \, du, \tag{A 6}$$

it can be concluded that the Melnikov function for the system with memory can be well approximated by the expression given in (3.7). This, of course, depends on finding an auxiliary linear system whose output provides a good match for the memory function. That procedure is described in Appendix B.

### Appendix B. The extended state space model for the radiation force

The radiation force is proportional to the convolution integral

$$\beta_1(\tau) = \int_{-\infty}^{+\infty} K(\tau - u) \dot{\phi}(u) \, du. \tag{B 1}$$

It is to be approximated as an output of an  $n$ th-order linear system with  $\dot{\phi}(\tau)$  as its input. The form of this equation is taken to be

$$\left[ a_{n+1} \frac{d^n}{d\tau^n} + a_n \frac{d^{n-1}}{d\tau^{n-1}} + a_{n-1} \frac{d^{n-2}}{d\tau^{n-2}} + \dots + a_2 \frac{d}{d\tau} + a_1 \right] \beta_1 = \dot{\phi}. \tag{B 2}$$

As pointed out in § 5, there are several linear systems able to model this radiation moment, given by different orders and coefficients in the linear differential operator. Taking the Fourier transform of both sides yields the transfer function of (B 2),

$$\frac{B_1(\omega)}{\Phi_d(\omega)} = 1 \bigg/ \sum_{k=1}^{n+1} a_k (i\omega)^{k-1}, \quad (\text{B } 3)$$

where  $B_1(\omega)$  and  $\Phi_d(\omega)$  are the Fourier transforms of  $\beta_1(\tau)$  and  $\dot{\phi}_d(\tau)$ , respectively. From the Fourier transform of (B 1), we obtain

$$\frac{B_1(\omega)}{\Phi_d(\omega)} = 2\pi\mathcal{K}(\omega). \quad (\text{B } 4)$$

The Fourier transform of the memory function  $K(\tau)$  is given by (see, for example, Takagi *et al.* 1984)

$$\mathcal{K}(\omega) = B_{44}(\omega) - B_{44}(\infty) + i\omega(A_{44}(\omega) - A_{44}(\infty)). \quad (\text{B } 5)$$

Comparing these expressions for the transfer function, we obtain the relation

$$B_{44}(\omega) - B_{44}(\infty) + i\omega(A_{44}(\omega) - A_{44}(\infty)) = 1 \bigg/ \sum_{k=1}^{n+1} a_k (i\omega)^{k-1}, \quad (\text{B } 6)$$

which is equivalent to

$$\frac{(B_{44}(\omega) - B_{44}(\infty)) - i\omega(A_{44}(\omega) - A_{44}(\infty))}{\Gamma} = \sum_{k=1}^{n+1} a_k (i\omega)^{k-1}, \quad (\text{B } 7)$$

where

$$\Gamma = (B_{44}(\omega) - B_{44}(\infty))^2 + \omega^2(A_{44}(\omega) - A_{44}(\infty))^2. \quad (\text{B } 8)$$

By equating the real and imaginary parts of the two sides, we obtain two objective functions that are used for curving fitting. For example, the objective functions for  $n = 8$  are given by

$$a_9\omega^8 - a_7\omega^6 + a_5\omega^4 - a_3\omega^2 + a_1 = \frac{B_{44}(\omega) - B_{44}(\infty)}{\Gamma}, \quad (\text{B } 9)$$

$$a_8\omega^6 - a_6\omega^4 + a_4\omega^2 - a_2 = \frac{A_{44}(\omega) - A_{44}(\infty)}{\Gamma}. \quad (\text{B } 10)$$

It is frequently difficult to find polynomials which accurately fit (B 9) and (B 10), especially in the most useful frequency ranges ((0.0, 2.0) rad s<sup>-1</sup> in our case). The results of using the  $\chi^2$  fitting method (Press *et al.* 1992) are shown in figures 18 and 19 and table 3. The results vary significantly if different individual standard deviations  $\sigma_1$  are used in different frequency ranges. In ‘curve fit 1’, we set  $\sigma_i = 0.2, 1.0$  and  $\infty$  for  $\omega \in (0.0, 2.0), (2.0, 6.0)$  and  $(6.0, \infty)$ , respectively. In ‘curve fit 2’, we set  $\sigma_i = 0.2, 1.0$  and  $\infty$  for  $\omega \in (0.0, 2.0), (2.0, 3.0)$  and  $(3.0, \infty)$ , respectively. Neither of the two 9th-order polynomials fits the curves very well (see figures 18 and 19) and the  $a_i$  change significantly (table 3). In addition, the term  $1/a_{n+1}$  is of order  $10^{11}$  in ‘curve fit 1’ (and  $10^7$  in ‘curve fit 2’) while the other leading coefficients

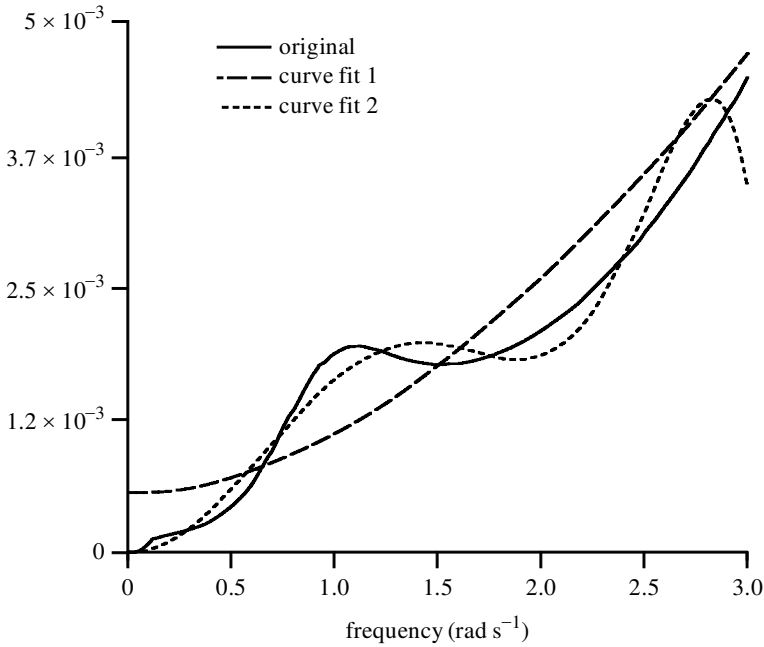


Figure 18. Curve fit for  $(B_{44}(\omega) - B_{44}(\infty))/\Gamma$  based on  $\chi^2$  fitting method.

in the system’s stiff matrix (equation (B 11)) are of order 1. This makes the range of relative magnitudes of the eigenvalues of the expanded system unacceptably large, which in turn makes numerical integration difficult, a common problem with this approach. Higher-order polynomials can achieve a better fit, but at some point the expanded system will be impossible to solve numerically. In addition, the cost spent on solving such a large system of equations will eventually exceed the cost of direct integration of the system with the memory function.

Once the size of the model has been determined and the values of the coefficients are obtained, the first-order form of the augmented dynamical system is given by

$$\begin{bmatrix} \dot{\phi} \\ \dot{\phi}_d \\ \dot{\beta}_1 \\ \dot{\beta}_2 \\ \vdots \\ \dot{\beta}_n \end{bmatrix} = \begin{bmatrix} 0 & 1 & 0 & 0 & 0 & \cdots & 0 \\ -\omega_n^2 & -b_{44}(\infty) & -C_\beta & 0 & 0 & \cdots & 0 \\ 0 & 0 & 0 & 1 & 0 & \cdots & 0 \\ 0 & 0 & 0 & 0 & 1 & \cdots & 0 \\ \vdots & \vdots & \vdots & \vdots & \vdots & \vdots & \vdots \\ 0 & \frac{1}{a_{n+1}} & \frac{-a_1}{a_{n+1}} & \frac{-a_2}{a_{n+1}} & \frac{-a_3}{a_{n+1}} & \cdots & \frac{-a_n}{a_{n+1}} \end{bmatrix} \begin{bmatrix} \phi \\ \phi_d \\ \beta_1 \\ \beta_2 \\ \vdots \\ \beta_n \end{bmatrix} + \begin{bmatrix} 0 \\ F_{nl}(\tau) \\ 0 \\ 0 \\ \vdots \\ 0 \end{bmatrix}, \tag{B 11}$$

where

$$\phi_d = \dot{\phi}, \quad b_{44}(\infty) = \frac{B_{44}(\infty)}{I_{44} + A_{44}(\infty)}, \quad C_\beta = \frac{1}{I_{44} + A_{44}(\infty)}$$

$$F_{nl}(\tau) = \frac{F(\tau) - B_{44q}(\omega)\phi_d|\phi_d| - \Delta(C_0 + C_3\phi^3 + \dots)}{I_{44} + A_{44}(\infty)}.$$

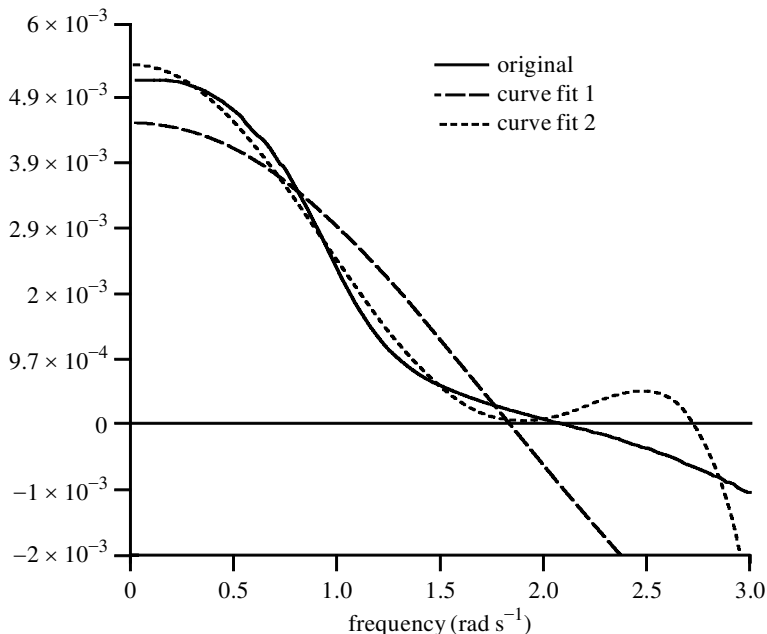


Figure 19. Curve fit for  $(A_{44}(\omega) - A_{44}(\infty))/\Gamma$  based on  $\chi^2$  fitting method.

Table 3. The deviation of curve fitting results with individual standard variations

|       | 'curve fit 1'              | 'curve fit 2'             |
|-------|----------------------------|---------------------------|
| $a_1$ | $5.57782 \times 10^{-6}$   | $-8.91987 \times 10^{-9}$ |
| $a_2$ | $-4.55531 \times 10^{-5}$  | $-5.42838 \times 10^{-5}$ |
| $a_3$ | $-5.72207 \times 10^{-6}$  | $-2.58928 \times 10^{-5}$ |
| $a_4$ | $-1.67755 \times 10^{-5}$  | $-3.74155 \times 10^{-5}$ |
| $a_5$ | $-2.03768 \times 10^{-7}$  | $-1.16985 \times 10^{-5}$ |
| $a_6$ | $-1.01694 \times 10^{-6}$  | $-8.27478 \times 10^{-6}$ |
| $a_7$ | $-9.19187 \times 10^{-9}$  | $-2.05076 \times 10^{-6}$ |
| $a_8$ | $-1.87369 \times 10^{-8}$  | $-5.68681 \times 10^{-7}$ |
| $a_9$ | $-4.30184 \times 10^{-11}$ | $-1.13707 \times 10^{-7}$ |

This is of the form required for the Melnikov theory of Appendix A, with  $\beta_1 = z_1$  and  $(\phi, \dot{\phi}) = (x, y)$ .

### References

Beck, F. B. & Troesch, A. W. 1990 *Documentation and user's manual for the computer program SHIPMO*. Department of Naval Architecture and Marine Engineering, The University of Michigan.

Bracewell, R. N. 1978 *The Fourier transform and its applications*, 2nd edn. New York: McGraw-Hill.

Cardo, A., Francescutto, A. & Nabergoj, R. 1981 Ultra-harmonics and sub-harmonics in the rolling motion of a ship: steady-state solution. *Int. Shipbuilding Prog.* **28**, 234–251.

- Cardo, A., Francescutto, A. & Nabergoj, R. 1984 Sub-harmonics oscillation in nonlinear rolling. *Ocean Engng* **11**, 663–669.
- Chen, S., Shaw, S. W. & Troesch, A. W. 1999 A systematic approach to modeling nonlinear multi-DOF ship motions in regular seas. *J. Ship Res.* **43**, 25–37.
- Cuong, H. T., Troesch, A. W. & Birdsall, T. G. 1982 The generation of digital random time histories. *Ocean Engng* **9**, 581–588.
- Esparza, I. & Falzarano, J. M. 1993 Nonlinear rolling motion of a statically biased ship under the effect of external and parametric excitations. In *Symp. on Dynamics and Vibration of Time-varying Systems, OE-Vol. 56, ASME*, pp. 111–122.
- Falzarano, J. M. & Zhang, F. 1993 Multiple degree of freedom global analysis of transient ship rolling motion. In *ASME Winter Meeting, Symp. on Nonlinear Dynamics, November*.
- Falzarano, J. M., Shaw, S. W. & Troesch, A. W. 1992 Application of global methods for analysing dynamical systems to ship rolling motion and capsizing. *Int. J. Bifurcation Chaos* **2**, 101–115.
- Francescutto, A. 1990 On the nonlinear motions of ships and structures at narrow band sea. In *Proc. IUTAM Symp. on Dynamics of Marine Vehicles and Structures in Waves, London*, pp. 291–304.
- Francescutto, A. 1992 Stochastic modelling of nonlinear motions in the presence of narrow band excitation. In *Proc. Int. Society of Offshore and Polar Engineering, San Francisco*, pp. 91–96.
- Frey, M. & Simiu, E. 1993 Noise-induced chaos and phase space flux. *Physica D* **63**, 312–340.
- Guckenheimer, J. & Holmes, P. 1983 *Nonlinear oscillations, dynamical systems, and bifurcations of vector fields*. Springer.
- Himeno, Y. 1981 Prediction of ship roll damping-state of the art. Report No. 239, Department of Naval Architecture and Marine Engineering, University of Michigan, Ann Arbor, Michigan.
- Holappa, K. W. & Falzarano, J. M. 1999 Application of extended state space to nonlinear ship rolling. *Ocean Engng* **26**, 227–240.
- Hsieh, S. R., Troesch, A. W. & Shaw, S. W. 1994 A nonlinear probabilistic method for predicting vessel capsizing in random beam seas. *Proc. R. Soc. Lond. A* **446**, 1–17.
- Huang, X., Gu, X. & Bao, W. 1994 The probability distribution of rolling amplitude of a ship in high waves. In *5th Int. Conf. on Stability of Ships and Ocean Vehicles, Melbourne, FL, USA*.
- Jiang, C. 1995 Highly nonlinear rolling motion heading to capsize. PhD Dissertation, Department of Naval Architecture and Marine Engineering, University of Michigan, Ann Arbor, Michigan.
- Jiang, C., Troesch, A. W. & Shaw, S. W. 1994 Nonlinear dynamics and capsizing of small fishing vessels. In *5th Int. Conf. on Stability of Ships and Ocean Vehicles, Melbourne, FL, USA*.
- Jiang, C., Troesch, A. W. & Shaw, S. W. 1996 Highly nonlinear rolling motion of biased ship in random seas. *J. Ship Res.* **40**, 125–135.
- Jiang, T., Schellin, T. E. & Sharma, S. D. 1987 Manoeuvring simulation of a tanker moored in a steady current including hydrodynamic memory effects and stability analysis. In *Proc. Int. Conf. On Ship Maneuverability, Royal Institution of Naval Architects, London*, vol. 1.
- McCreight, W. R. 1986 Ship maneuvering in waves. In *Proc. 16th Symp. on Naval Hydrodynamics, 1964*, pp. 3–128.
- Moon, F. C. & Li, G. X. 1985 Fractal basin boundaries and homoclinic orbits for periodic motion in a two-well potential. *Phys. Rev. Lett.* **55**, 1439–1442.
- Nayfeh, A. H. 1973 *Perturbation methods*. Wiley.
- Nayfeh, A. H. & Khdeir, A. A. 1986a Nonlinear rolling of ships in regular beams seas. *Int. Shipbuilding Prog.* **33**, 40–49.
- Nayfeh, A. H. & Khdeir, A. A. 1986b Nonlinear rolling of biased ships in regular beams waves. *Int. Shipbuilding Prog.* **33**, 84–93.
- Ogilvie, T. F. 1964 Recent progress toward the understanding and prediction of ship motions. In *5th Symp. On Naval Hydrodynamics, 1964*, pp. 3–128.
- Press, W. H., Teukolsky, S. A., Vetterling, W. T. & Flannery, B. P. 1992 *Numerical recipes in FORTRAN*. Cambridge University Press.

- Roberts, J. B. 1982 A stochastic theory for nonlinear ship rolling in irregular seas. *J. Ship Res.* **26**, 229–245.
- Roberts, J. B. & Dacunha, N. C. 1985 Roll motion of a ship in random beam waves: comparison between theory and experiment. *J. Ship Res.* **29**, 112–126.
- Senjanović, I. 1994 Harmonic analysis of nonlinear oscillation of cubic dynamical systems. *J. Ship Res.* **29**, 112–126.
- Spyrou K. J. 1996 Dynamic instability in quartering seas: the behaviour of a ship during broaching. *J. Ship Res.* **40**, 46–59.
- Spyrou K. J. & Umeda, N. 1995 From surf-riding to loss of control and capsize: a model of dynamic behaviour of ships in following/quartering seas. In *Sixth Int. Symp. on Practical Design of Ships and Mobile Units (PRADS)*, Seoul, Korea, 1 September.
- Takagi, M., Saito, K. & Nakamura, S. 1984 Comparisons of simulation methods for motions of a moored body in waves. In *3rd ASME OMAE Symp., New Orleans*, pp. 214–224.
- Thompson, J. M. T. 1989*a* Loss of engineering integrity due to the erosion of absolute and transient basin boundaries. In *Proc. IUTAM Symp. on the Nonlinear Dynamics in Engineering Systems*.
- Thompson, J. M. T. 1989*b* Chaotic phenomena triggering the escape from a potential well. *Proc. R. Soc. Lond. A* **421**, 195–225.
- Thompson, J. M. T. 1990 Transient basins: a new tool for designing ships against capsize. In *Proc. IUTAM Symp. on the Dynamics of Marine Vehicles and Structures in Waves, London*, pp. 325–331.
- Thompson, J. M. T. 1997 Designing against capsize in beam seas: recent advances and new insights. *Appl. Mech. Rev.* **50**, 307–325.
- Umeda, N. & Renilson, M. R. 1994 Broaching of a fishing vessel in following and quartering seas—nonlinear dynamical systems approach. In *Fifth Int. Symp. on the Stability of Ships and Ocean Vehicles, Melbourne, FL, USA, November*.
- Vassalos, D. & Spyrou, K. 1990 An investigation into the combinend effects of directional and transverse stabilities. In *Fourth Int. Symp. on the Stability of Ships and Ocean Vehicles, Naples, Italy*, pp. 519–527.
- Vassalos, D., Umeda, N., Hamamoto, M. & Tsangaris, M. 1999 Modelling extreme ship behaviour in astern seas. *R. Inst. Naval Architects* (Winter Meeting).
- Virgin, L. N. 1987 The nonlinear rolling response of a vessel including chaotic motions leading to capsize in regular seas. *Appl. Ocean Res.* **9**, 89–95.
- Virgin, L. N. 1989 Approximate criterion for capsize based on deterministic dynamics. *Dyn. Stability Systems* **4**, 55–70.
- Warwick, K. 1989 *Control systems*. Englewood Cliffs, NJ: Prentice-Hall.
- Wiggins, S. 1990 *Introduction to applied nonlinear dynamical systems and chaos*. Springer.
- Wiggins, S. 1992 *Chaotic transport in dynamical systems*. Springer.
- Wright, J. H. & Marshfield, W. B. 1980 Ship roll response and capsize behaviour in beam seas. *Trans. R. Inst. Naval Architects* **122**, 129–148.